Materials Advances

ROYAL SOCIETY OF CHEMISTRY

REVIEW

View Article Online
View Journal | View Issue

Cite this: *Mater. Adv.*, 2022, 3, 4103

Challenges surrounding nanosheets and their application to solar-driven photocatalytic water treatment

Diego T. Pérez-Álvarez,†*[a] Jacob Brown,[a] Elzahraa A. Elgohary,[b] Yasser M. A. Mohamed,[b] Hossam A. El Nazer,[b] Philip Davies[a] and Jason Stafford*[a]

Received 10th March 2022,
Accepted 24th April 2022

DOI: 10.1039/d2ma00276k

rsc.li/materials-advances

Industrialisation has deepened the water crisis in arid climates, where wastewater runoff from heavy industry has polluted groundwater sources so heavily that traditional methods of water treatment have proven ineffective. Photocatalysis is an emerging technology which has the potential to treat water using only sunlight, but is unrealised using traditional, inefficient photocatalysts (*e.g.* TiO_2). Recently, a slew of visible light active 2D nanomaterials such as MoS_2 and g-C_3N_4, have shown great promise, with others playing an essential supporting role in larger composites (*e.g.* graphene). Scalable synthesis of these nanosheets has remained elusive, as they require careful synthesis tailored towards their role within a photocatalytic composite. Along with recovering the nanosheets post-treatment, these remain the greatest challenges barring the adoption of these materials more generally. Through this review, we find that research into nanosheet-based photocatalysis should focus on developing materials from a systems level perspective, with careful consideration taken to how the material presented is to be applied in clean water technologies and synthesised from its base components.

1 Motivation

Increasing populations, weather extremes and rapid industrialisation (with poor regulation) has led to a scarcity of clean water sources in many developing countries, rendering them unsuitable even for irrigation.[1] This is especially true in arid, drought-prone climates, where intermediate water sequestration systems like dams and rainwater catchment are less relevant. Egypt's freshwater consumption for example, is much greater than its freshwater production, and with the extra competition for water upstream of the Nile, the crisis here is only set to deepen in the short term.[2,3] The WHO estimates that although the number of people who have access to water has increased since the millennium, most are drinking from polluted sources, with an estimated three out of every ten people lacking access to clean water.[5] In this vein, it is paramount to develop cost-efficient methods of water treatment, especially for arid climates.

Traditional methods of water treatment often struggle with the diversity of contaminants in such highly polluted waters. Chlorination for example has always been problematic, as it ends up creating even more toxic by-products;[4] other chemical treatments have historically been avoided due to mass-scale unforeseen medical consequences.[6] Traditionally, coagulation or adsorption are used, but by their nature simply concentrate the contaminants which remain after processing.[7] Membrane filtration systems have consistently suffered from complicated issues stemming from the fouling of the membranes and inefficient removal of pollutants,[8] leading to increased costs incurred by using progressively smaller meshes from ultra-filtration to reverse-osmosis.

In the context of a small community, SOlar water DISinfection (SODIS) has been touted by the WHO for its passive ability to clean water; where post filtering, it takes 6 hours under less than 50% cloud cover to produce clean drinking water. This process requires low turbidity water, and kills pathogens owing to a combination of Ultra-Violet light (UV)-induced DNA damage, thermal inactivation, and photo-oxidative destruction.[9] Some heavier pollutants such as dyes and metals require excessively long exposure for inactivation, and much more intense treatment for timely remediation.

Photocatalysis is one of a subset of Advanced Oxidation Processes (AOPs)[10] which are able to hasten the natural degradation of these heavier pollutants by using light to catalyse the reactions directly,[11,12] along with its own antimicrobial effect.[13]

[a] *School of Engineering, University of Birmingham, UK. E-mail: d.t.perez-alvarez@bham.ac.uk*
[b] *Photochemistry Department, National Research Center, Dokki, Giza, 12622, Egypt. E-mail: j.stafford@bham.ac.uk*
† Primary author.

This degradation pathway has been examined using gas chromatography techniques, revealing phenols as the main degradation intermediary (for Methylene Blue), which subsequently break down into CO_2 and H_2O.[14,15] Photocatalysts (PCs) have been successfully applied to many fields beyond water treatment, from water splitting,[16–18] the production of ammonia through N_2 fixation,[19–21] to the reduction of CO_2 into synthetic fuels.[22–26]

Conventional renewables can also be used to power high energy light sources for photocatalysis, which can be tailored to suit the activation range of a particular photocatalyst, whilst simultaneously degrading pollutants by direct UV excitation and allowing treatment to continue at night.[27] The primary byproducts of photocatalytic water treatment are CO_2 and H_2O.[28] Notably, hydrogen, a sustainable fuel source, is another byproduct that can be produced in reasonable quantities if the catalyst is optimised.[29,30] This is beneficial as hydrogen from pollutant degradation is more thermodynamically favourable than from photocatalytic water splitting,[29] making use of would be waste products.

Photocatalytic systems offer benefits on many levels, as an inherently clean, low-cost and environmentally friendly solution to many of these problems.[31] The cutting edge of photocatalytic research focuses on novel, Visible Light Active (VLA) PCs, which rely heavily on nanomaterial composites, especially those based on 2D nanosheets. Since their application to photocatalysis, it has been difficult to intensify the procedure, as a number of life cycle considerations remain unaddressed:[32]

- Production – particularly towards 2D PCs. They are difficult and expensive to produce which currently make them impractical at scale.
- Application – it is not clear what is best practice in applying PCs at scale, especially 2D PCs.
- Recovery and reuse – by virtue of their size, nanomaterials represent an intrinsic difficulty to separate photocatalyst from solute post treatment.

From rooftop to industrial scale setups, solar-driven photocatalysis has the potential to fundamentally change the way water treatment is realised. Fig. 1 provides a visualisation of areas that would benefit the most from widespread adoption of such a technique. Many Middle-Eastern to northeast African countries are currently experiencing an extremely high strain on their freshwater resources, with Egypt in excess of 1000%. They also experience a high amount of solar radiation, making them a prime candidate for solar photocatalysis.

Clean drinking water is a global problem, which will only come to affect more people. New technologies are essential to keep pace with human and climate developments. The discovery of efficient and generalised methods of preparing, applying and reusing PCs would open the door to this new industry, providing cheap and accessible freshwater to many of the regions which need it the most.

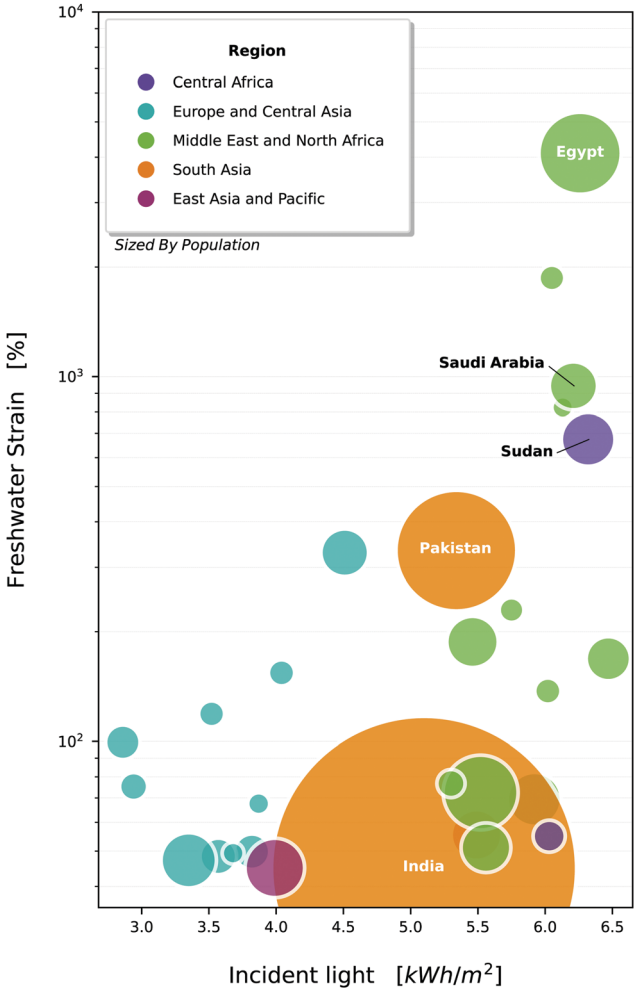

Fig. 1 Countries of the world, plotted against their strain on freshwater resources[1] and average daily incident light.[33] Bubbles are sized by population, and coloured by economic area denoted by the world bank. Selected countries are all experiencing withdrawals above 40% (high water stress), and have a population >5 million, though data is not available for all countries. Note that withdrawals exceed 100% in a number of countries, which indicates that the local freshwater is being sourced unsustainably (*e.g.* from aquifers) or heavy use of desalination.

2 Introduction

Since the discovery of the photocatalytic properties of TiO_2 in 1972,[35] photocatalytic materials have garnered attention due to their thermal stability, biocompatability and sustainability.[31] In the wake of TiO_2 other metallic powders such as WO_3, ZnO and Bi_2O_3 have all demonstrated the photocatalytic effect to varying degrees.[36–39] TiO_2 has gone on to moderate success as the only commercially available PC (P25-degussa), though it has not broken into the the water treatment sector due to its low efficiency and difficult recovery.

The general photocatalytic process for semi-conducting materials can be described as follows. An incident photon with energy greater than or equal to the PC band gap can excite electrons from the valence band to the conduction band creating an electron-hole pair.[40,41] This electron-hole pair can interact with adsorbed compounds to directly degrade pollutants, or to generate redox species capable of degrading organic pollutants into CO_2, water, and mineral acids.[42–44] It is generally agreed that the oxidative $^{\bullet}OH$ degradation pathway is dominant.[44] A schematic

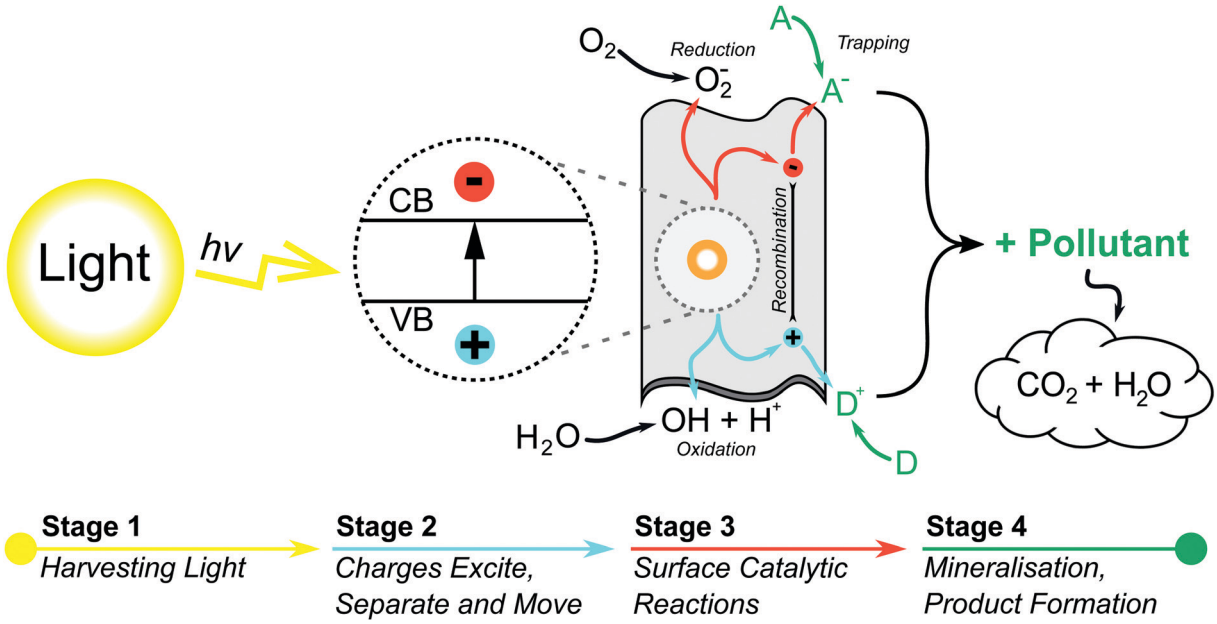

Fig. 2 A schematic diagram for a heterogenous photocatalytic process over a 2D photocatalyst surface, detailing some of the many reactions that can occur to pollutants through the use of photogenerated charge carriers. (A and D) Represent the surface adsorbed acceptor and donor species respectively.[34]

representation of this process is given in Fig. 2 for a 2D nanosheet, and more detail on the reaction mechanisms in Section 4. The inability to use visible light in legacy bulk PCs stems from the large band gap required for excitation, but even when excited they are invariably inefficient, owing for the tendency of electron-holes to recombine at any point as they migrate to activation sites on the surface of the photocatalyst.[45]

Novel developments in nanomaterials with tunable geometries have, however, opened new avenues of experimentation. What is striking about these materials is the diversity of structures they can take, from 0D nanospheres[46,47] to 1D nanorods/nanotubes[48–51] and 2D nanosheets.[52–55] Regardless of morphology, nano-scale PCs outperform their bulk counterparts in all cases.[56] Of these structures, many behave completely differently in terms of photocatalysis, and 2D nanosheets in particular offer some unique advantages arising from their structure.

(1) They have a large surface area per amount of material, maximising the space available for photocatalytic reactions.
(2) Their ultra-thin nature reduces the migration distance for electrons and holes to reach active sites, increasing the efficiency of photocatalytic reactions and reducing the possibility of electron-hole recombination.

Nowadays, there is a large body of research discussing the nanostructure of PCs, and it is clear that these materials offer a much better solution than their bulk counterparts. To give an example, TiO_2 nanosheets show an increase in activity when compared to their bulk phase counterparts, accompanied by a change in their band gap.[12] Li *et al.*[57] provides a comprehensive review into the design of these 2D based PCs, including many of the different construction strategies for tuning a PC's activity under different wavelengths of light. In the stride to boost catalytic performance, many researchers have taken to doping graphene and 2D materials using a variety of material sources.[58] Even so, the literature tends to point towards a 2D atomic structure being the main component in the design of future PCs.

In essence, the lack of more widespread use of nanoscale PCs is due to the high synthesis and characterisation cost these materials entail. Take graphene as an example, at the time of writing 100 g of current commercial few-layer graphene costs within the region of € 200. This, coupled with the fact that only 20% of commercial sources consist of true mono to few layered graphene[59] hints at the great difficulty that the synthesis of 2D materials entails. Production intensification and international standards for graphene[60] offer a pathway to a wide range of commercial composites with reliable and remarkably enhanced photocatalytic activity, such is its prevalence within photocatalysis.[61] Importantly, 2D semiconductors that support solar-driven photocatalysis (*e.g.* MoS_2 nanosheets) currently have less commercial focus than graphene-based materials. This impacts on the availability and cost of high quality 2D materials for use in large-scale water treatment.

Table 1, provides a summary of a number of different cost estimations for photocatalytic reactors, which demonstrates how much more expensive they are when compared to current methodologies costing near € 0.39 m^{-3} on average,[65] (dependant on the original contamination of the groundwater source). These sources nearly all use the commercial P25-degussa,[66] which is non-optimal. The use of more efficient nano-composite PCs would dramatically improve efficiency across the board. Lowering the cost of these materials requires high-throughput methods of synthesis, but this cannot come at the expense of quality, as nanosheet quality is intrinsically linked to its performance. Because of this, both aspects are looked at in parallel in Section 5.

Table 1 Operating cost values from literature (€ m^{-3}), with stated prices adjusted for inflation

Catalyst	Notes	Cost	Ref.
TiO_2 – P25 slurry reactor	Measured the destruction of pesticides EPTC, butiphos and γ-lindane beginning at concentrations of 500 μg L^{-1} and ending at their maximum permissible level (0.1 μg L^{-1}), and the four-log inactivation of *E. faecalis* bacteria. Tested using a 500 m^2 CPC array with a calculated capacity of 42 L h^{-1} m^{-2}.	1.1	62
TiO_2 – P25 slurry reactor	Measured the complete removal of ECs (emerging contaminants, includes a wide variety of compounds such as pharmaceuticals, personal care products, hormones, industrial additives and household chemicals, with most ECs not yet regulated.) and 20% reduction in TOC (total organic carbon) levels. Tested with a 0.25 m^2 CPC array at a maximum of 24 L min^{-1}, in semi-batch operation.	TOC: 2.14 EC: 2.87	63
TiO_2 coated rotating drum reactor	Illuminated by a combination of artificial UV lights and solar radiation. Specific enhancing conditions such as the acidic pH 4 and presence of H_2O_2 at 250 mg L^{-1} noted. Measured the removal of 10 mg L^{-1} aniline solution in deionised water (100% after 10 minutes), and the removal of TOC (85% after 120 minutes).	0.72	64

Material synthesis is only part of the problem; in reality, the full life cycle of the photocatalyst must be examined, and as suggested before, the issues surrounding the application of these materials are as prevalent. Hence, there has been a push to evaluate the effectiveness of PCs at large scale, beginning with two small pilot plants in Morrocco and Spain.[67] These examined a range of different techniques, but centered on employing Compound-Parabolic-Concentrators (CPCs) to maximise the incident light intensity.[68] Since the turn of the millennium, pilot plants such as these have begun to appear with greater frequency and complexity (complete with 1–2 axes solar tracking), mainly due to funding by the EU through projects such as SOLWATER and AQUACAT.[69]

These pilot facilities have invariably used bulk PCs, as opposed to atomic scale materials, and therein circumvent one of the large issues surrounding nano-scale PCs; PC removal/recovery.[71] Separation of a nano-scale photocatalyst implies the post-process is as laborious as some of the aforementioned nano-filtration techniques, if standard methods are used. This suggests that the ideal photocatalytic material must have some thought for its reuse. This could either be intrinsic to the photocatalyst material itself, or through some external implementation. This opens up other methods of application, such as photoelectrocatalysis,[72] where the photocatalyst is held within an anode, in contact with the water but not allowed to mix directly. This makes practical sense at a cost to efficiency,[73] implying that the ideal implementation is one that looks at photocatalysis as an entire process when designing a PC, thereby ensuring that the material developed covers both efficient and practical application.[74,75] A holistic consideration of these trade offs is an essential part of selecting a suitable photocatalytic system.

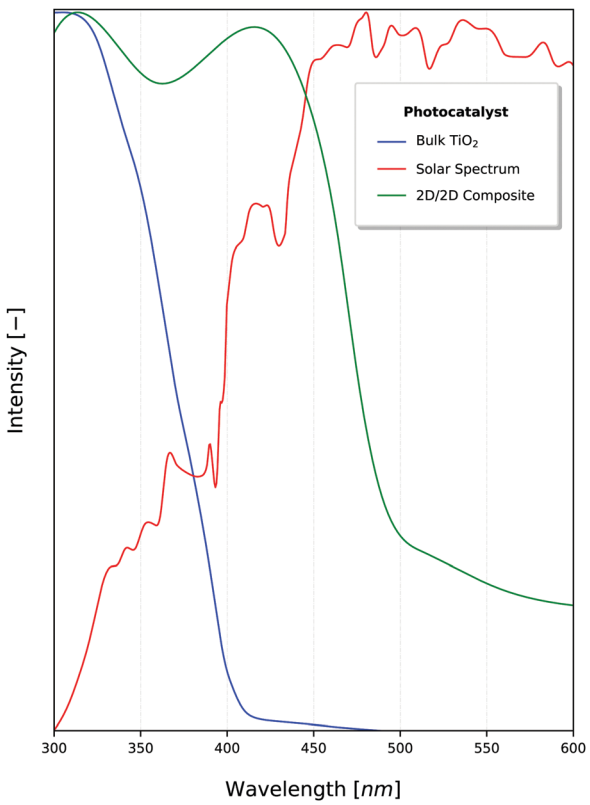

Fig. 3 Intensity of sunlight (red) in juxtaposition to the photocatalytic activation (normalised) of TiO_2[67] and a 2D nanocomposite constructed using graphitic carbon nitride (g-C_3N_4).[16] A total of 46% of the solar energy falls within the visible light range.[70]

3 2D photocatalysts

2D materials are traditionally best known for their enhanced mechanical, optical and electrical properties.[76,77] They have been rising steadily in popularity along with other low-dimensional materials due to their enhanced photocatalytic properties, which have been under investigation even before the discovery of graphene in 2004.[78,79] The benefits of nano-structure PCs stem primarily from the enhanced surface area available per amount of material. Though 0D & 1D PCs maximise these properties,[80] 2D materials are able to effectively utilise incident sunlight because of their light-scattering properties (Fig. 3), with the absorption and band gap being dependant on the depth of light penetrated.[12,81] This also means that the number of atomic layers (or equivalently, the thickness) of these 2D materials is critical to the effective absorption of 2D PCs,[82] as shown in Fig. 4.

The rise in publications shown in Fig. 5, describes the current prominence of nanosheets within research. Interestingly, most hits for unfiltered patents are false positives, and most simply are patenting a specific material and its method of production. This is slightly disingenuous, as generalised

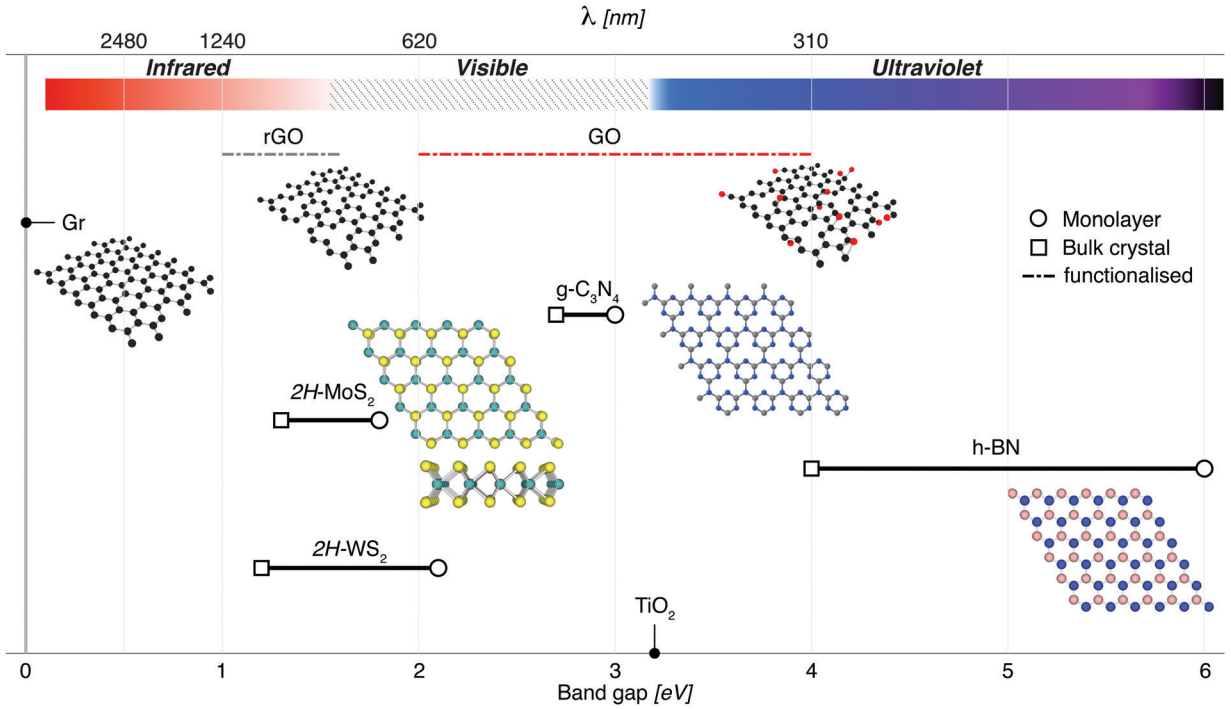

Fig. 4 2D materials which have been a focus for photocatalysis research include g-C_3N_4, transition metal dichalcogenides such as MoS_2, insulators such as h-BN for composites, and other graphene-related materials (Gr, rGO and GO). Apart from graphene, which has a zero band gap, these materials can be exfoliated from their bulk materials to engineer nanosheets with a direct band gap. In the case of rGO and GO, modifications to the band gap are made possible by removing/adding functional groups. TiO_2 has been included for reference, illustrating the advantages of narrow band gap nanosheets that can target visible wavelengths for solar-driven photocatalysis. For g-C_3N_4, a triazine structure is shown inset. This material also has an heptazine structure which is shown in Fig. 8.

methodologies for the application of photocatalytic substances is prominent throughout patent searches, simply that few target the nano-scale PCs in particular. This principally demonstrates the lag between research and industrial uptake, but also tells of how important the synthesis route is to these PCs, as it effectively determines how the catalyst is to be used and reused.

The range of materials discovered so far only scratches the surface of a variety of naturally occurring materials held together by van der Waals forces,[83–85] and with novel developments in computational pre-screening of materials in terms of photocatalytic activity,[86,87] highly-active PCs can be found at an astonishing rate. The most active of which typically work in conjunction with other PCs in the form of composites.[88,89] In fact, the search in Fig. 5 found that one-third of all hits on articles/papers were directly examining functional composites of several different materials to improve photocatalytic activity.

Composites themselves vary dramatically in terms of structure and functionality. On an individual level, the dimensionality of a photocatalyst is clearly important (as discussed in Section 2), but compositing adds a level of inter-dependency between dissimilar materials which brings dimensionality to the fore.[90] At this point, interfacing between dissimilar materials can critically impact photocatalytic activity, for instance by altering the transfer rate of charge carriers between co-catalysts. 2D materials are again naturally suited to this, as they exhibit a large specific surface area, which gives reason for the rise in 2D/2D (one 2D material layered over another different 2D material) heterostructures.[25,91,92]

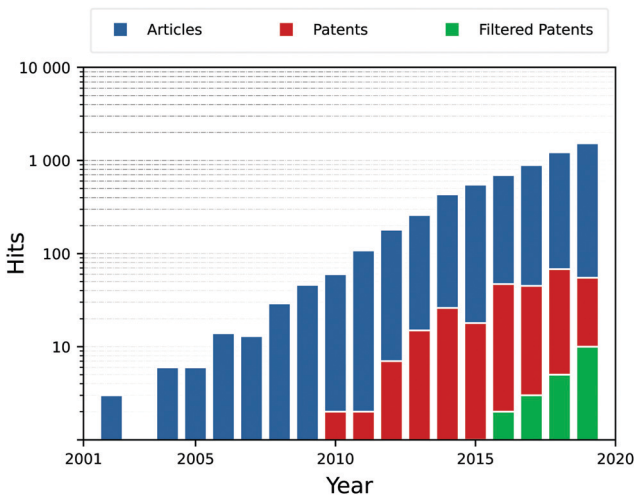

Fig. 5 Search hits for "photocatalysis" and ("2D" or "nanosheet"), filtered or unfiltered for synthesis synonyms (synthesis, construction, preparation). This shows the exponential rise in popularity of 2D PCs, particularly in their synthesis. Search terms were applied to the Title and abstract of publications. At the time of writing, 2020 and 2021 figures are yet to stabilise as publications are still under review for release. Data accessed through the Web of Knowledge and the European Unions' Espacenet.

As an example, most PCs can be doped with graphene[61] to enhance the separation of charge carriers from the parent photocatalyst, and in this regard graphene outperforms carbon nanotubes.[93] The same study reported the highest activity using 2D/2D titania-graphene nanosheet structures. This demonstrates a type II Heterostructure, which due to their differing band gaps promote the movement of charge carriers between the titania and graphene. These types of heterostructures in particular have been rising in prominence because of this charge separating interaction.[94,95]

Though metal oxides have been extensively researched as one of the first consistently active photocatalytic materials, other categories have been found which demonstrate good photocatalytic activity. Transitional Metal Dichalcogenides (TMDs) being the most notable,[12,53,96] as they exhibit similar or even better absorption of light, with MoS_2 nanosheets having suitable band-gap structure (1.35–1.8 eV[97]) for the absorption of visible light.[98] Even graphene, a zero band-gap material that is inactive by itself, can be functionalised by nitrogen doping (and other dopants) to work as a visible light photocatalyst.[99,100] Functionalised graphene (GO, r-GO) makes up a small portion of a large number of non-metal based PCs. The most prominent non-metal is g-C_3N_4,[101,102] belonging to a larger group of Covalent Organic Frameworks (COFs).

This is by no means an exhaustive list, and other nanosheet materials and their composites used in wastewater treatment are presented in Table 2. Furthermore, linking computational pre-screening techniques for photocatalytic activity[86,87,103] with large explorational studies of layered materials held together by van der Waals forces[83,85] provides the possibility to find new, exciting materials which have not been synthesized as of yet.[104]

The morphology of these nanosheets is often as important as the type of photocatalyst itself. In bulk PCs, the crystalline structure affects photocatalytic performance, as demonstrated by the difference in activity between the different crystalline structures of TiO_2.[105,106] In 2D materials, oxidising graphene into Graphene Oxide (GO) or introducing defects along the edges or basal plane is known to affect the electron mobility of the sheets and indeed their photocatalytic activity.[107–110] Inclusions are commonly introduced during synthesis, and exemplify the importance of maintaining reliable production techniques which are also scalable. The search for scalable synthesis is what first gave rise to GO and its variants, accentuating the great difficulty in creating pristine nanosheets.[59] Thus the synthesis route plays a key role, impacting morphology, defect density, and ultimately, photocatalytic performance.[111]

4 Photocatalysis mechanisms

As discussed briefly in the introduction photocatalysis occurs when a semiconductor is irradiated by a photon with energy greater than or equal to its band gap in order to produce an electron-hole pair which can interact with adsorped molecules to create redox couples (Fig. 2) or directly degrade adsorped pollutants. There are a number of techniques used to enhance the creation of redox couples such as heterojunctions, doping, reducing the material morphology to the nanoscale (Fig. 4), and defect engineering.

This article is not intended to serve as a comprehensive review of these mechanisms and there are several articles which cover these topics in greater detail. Li *et al.* produced a detailed review of charge recombination including heterojunctions, electron donors, and spin polarisation regulation.[140] Although somewhat dated now, Wang *et al.* provided a thorough introduction to heterojunction photocatalysts.[141] In a recent review from a different group of authors, Wang *et al.* included detail on different classifications of semiconductor materials, heterojunctions and photocatalysis applications.[142] For information regarding active sites, although not specific to photocatalytic water treatment, Low *et al.*,[143] Bo *et al.*,[144] and Li *et al.*[145] Finally, Serrá *et al.* have written a comprehensive review of photocatalytic treatment of natural waters including a summary of the reactions which take place to generate redox species, and the effects of environmental conditions such as solution pH.[146] These reactions are summarised as follows:

$$H_2O + h^+ \rightarrow {}^\bullet OH + H^+ \quad (R1)$$

$$O_2 + e^- \rightarrow O_2^{\bullet -} \quad (R2)$$

$$H_2O_2 + e^- \rightarrow {}^\bullet OH + OH^- \quad (R3)$$

where $^\bullet$OH is the highly oxidising species, hydroxyl radical, and $O_2^\bullet$ is the weak oxidant, superoxide. The H_2O_2 in (R3) comes from the $O_2^{\bullet -}$ from (R2) reacting with H^+[147] (R4 and R5).

$$O_2^{\bullet -} + H^+ \rightarrow HO_2^\bullet \quad (R4)$$

$$HO_2^\bullet + HO_2^\bullet \rightarrow H_2O_2 + O_2 \quad (R5)$$

Reactions which include the addition of e^- (R2 and R3) occur at the conduction band of the semiconductor, and reactions involving h^+ (R1) occur at the valence band. The generated oxidising species ($^\bullet$OH, $O_2^{\bullet -}$) can go on to degrade pollutants (R6).

$$\text{Pollutant} + {}^\bullet OH/O_2^{\bullet -} \rightarrow H_2O + CO_2 + H \quad (R6)$$

Reaction (R2) requires the donation of a photoexcited electron from the semiconductor to the O_2. This electron has a minimum energy of −0.33 V *vs.* NHE[142,148,149] (normal hydrogen electrode). If the energy level of the photocatalyst conduction band is not sufficiently low (<-0.33 V) then the reaction will not take place. Similarly, reaction (R1) requires the H_2O to donate an electron to the valence band of the semiconductor in order to fill the h^+ formed during photoexcitation. If the valence band energy level is too negative (<2.32 V[142,148,149]) this reaction will not occur.[150] This is illustrated in Fig. 6.

4.1 Heterojunctions

For efficient solar photocatalysis it is preferential to decrease the band gap energy such that a larger proportion of the solar spectrum can be used for the excitation of electrons and thus creation of redox couples. This reduced band gap comes at the cost of reduced oxidation and or reduction potentials.[152]

Table 2 A range of nanosheet photocatalysts and composites, their production methods, and application in water treatment

Photocatalyst	Water contaminant	Radiation source	Photocatalytic reaction results	Ref.
Hydrothermal method (HT)				
TiO_2-GO	Methylene Blue (MB)[d]	Visible light, solar simulator (100 mW cm^{-2})	MB concentration fraction after 80 min: 0.20 for TiO_2 NW-GO 0.56 for TiO_2 NP-GO	112
rGO/Pd/TiO_2	Rhodamine B (RhB)[d]	UV light, 400 W mercury lamp	RhB degradation % after 40 min with 0.03 g catalyst and 10 ppm dye initial concentration: 79% for rGO/Pd/TiO_2-NPs 90% for rGO/Pd/TiO_2-NWs, after 5 cycles photocatalyst was stable with slight decrease in degradation %.	113
WO_3/rGO	Methylene Blue (MB)[d]	Visible light, 300 W xenon lamp	83% dye degradation % within 70 min, 20 mg catalyst and 10 mg L^{-1} dye.	114
Boron-doped TiO_2/GO	Bisphenol A (BPA)	Visible light, 300 W xenon lamp	47.66% BPA degradation % after 4 h with GO amount equal to 2% of titania mass.	115
ZnO–TiO_2/rGO	Methylene Blue (MB)[d]	UV light, TUV 11W	99.83% MB degradation after 120 min at pH 9 with 40 mg catalyst and 20 mg L^{-1} MB.	116
WO_3/rGO	Rhodamine B (RhB)[d] ciprofloxaxin (CIP) antibiotic	Visible light, 300 W metal halide lamp	96% RhB and 90% CIP degradation for WO_3/rGO-40 photocatalyst after 120 min with 20 μM pollutant, 20 mg L^{-1} catalyst.	117
g-C_3N_4	Rhodamine B (RhB)[d] tetracycline (TC) antibiotic	Visible light, 300 W xenon lamp	100% RhB degradation rate after 15 min 100% TC degradation rate after 60 min with 20 mg catalyst and 20 mg L^{-1} pollutant.	118
Solvothermal method (ST)				
Ag/GO/TiO_2	Paraoxon pesticide	Visible light, 570 W xenon lamp	Nanocomposite with 6 wt% Ag and 1 wt% graphene content has the best photocatalytic activity and showed 100% TOC removal after 110 min with 31 mg L^{-1} pesticide and 0.2 g L^{-1} catalyst.	119
g-C_3N_4 fluorine doped/g-C_3N_4 (F-CNS)	Rhodamine B (RhB)[d]	Visible light, 500 W xenon lamp	Degradation rate of RhB by F-CNS was 1.6 times that of CNS after 2 h with 30 mg of catalyst, 10 mg L^{-1} dye.	120
MoS_2/CdS	Methylene Orange (MO)[de]	Visible light, 350 W xenon lamp	100% MO degradation rate by MoS_2/CdS 1–220 (1 : 1 molar ratio prepared at 220 °C) within 60 min with 30 mg L^{-1} dye and 60 mg catalyst.	121
$MnFe_2O_4$/graphene sand composite (GSC)	Methylene Blue (MB)[d]	Sunlight irradiation[b]	100% MB degradation rate after 180 min with 10 mg L^{-1} of MB and 0.25 g L^{-1} catalyst at pH 7.65 in presence of 5 mL of H_2O_2	122
ZnO/GO	Neutral red (NR)[d] crystal violet (CV)[d] congo red (CR)[d] methyl orange (MO)[d]	UV-light, 40 W	Dye degradation % with 400 mg L^{-1} catalyst and 10 ppm dye was: 100% NR after 20 min, 97% CV after 80 min, 68% CR after 150 min, 66% MO after 150 min.	123,124
Self-assembly method				
GO/CdS	*Escherichia coli* (*E. coli*) *Bacillus subtilis* (*B. subtilis*) Acid Orange 7 (AO7) Rhodamine B (RhB)[d] photoreduction of $Cr6^+$	Visible light, solar light simulator (100 mW cm^{-2})	100% of both *E. coli* and *B. subtilis* were inactivated within 25 min with 5 mg catalyst. 80% AO7 and 90% RhB were degraded within 60 min by 20 mg catalyst and 20 mg L^{-1} dye. 70% Cr^{6+} was photoreduced after 120 min and 15 mg catalyst.	125
γ-Fe_2O_3/GO	Methylene Blue (MB)[d]	UV irradiation, 250 W high pressure Hg lamp	100% MB degradation after 80 min with 10 mg of catalyst and 50 mg L^{-1} dye.	126
SnO_2/rGO	Methylene Blue (MB)[d]	Sunlight Irradiation[b], Tiruchirappalli city, August	100% MB disappearance by SnO_2 : rGO (1 : 3 ratio) at less than 3 minutes with 20 mg of catalyst and 5ppm MB. Rapid disappearance is noted to be due to the effective adsorption properties of SnO_2 : rGO (1 : 3).	127

Table 2 (*continued*)

Photocatalyst	Water contaminant	Radiation source	Photocatalytic reaction results	Ref.
Co-precipitation method				
Fe_3O_4/graphene/sulfur-doped g-C_3N_4 (Fe_3O_4/GE/SCN)	Ranitidine drug N-nitrosodimethylamine (NDMA)	Visible light, 300 W xenon lamp	100% ranitidine removal and 57.3% reduction in NDMA formation potential by 20%-Fe_3O_4/GE/SCN composite after 60 min with 1 g L^{-1} catalyst and 2 mg L^{-1} pollutant initial concentration at pH 7.0	128
Chemical vapor deposition (CVD) technique				
Graphene	Rhodamine B (RhB)[d] Janus Green (JG)[d]	Sunlight irradiation[b]	Graphene nanosheets (GNS) synthesized from black carbon collected from diesel engine. 98.65% RhB and 96.34% JG degraded by GNS after 120 minutes with 0.90 g L^{-1} catalyst and 10 mM dye at pH = 6.	129
Ag/ReS_2	*Escherichia coli* (*E. coli*)	Visible light[c]	Complete inactivation of *E. coli* within 30 min by Ag(3)/ReS_2 with 1.72 mg L^{-1} catalyst and 104 CFU per mL *E. coli.* After 5 consecutive cycles the photocatalytic disinfection performance for the photocatalyst is not reduced.	130
Graphene/anatase-TiO_2 (G/a-TiO_2)	Methyl Orange (MO)[d]	UV light, 250 W high-pressure mercury lamp	88% MO degradation rate by bilayer G-60/a-TiO_2 composite after 40 min with 10 mg catalyst and 12.5 mg L^{-1} dye	131
Sonication-photo-biosynthesis combined method				
Ag/Au/rGO	Red sea water sample[a]	Visible light, halogen lamp	An ultra-pure water is obtained with zero micro-organisms (HPC), salts, TDS, and Total hardness at pH = 7 after 5 h irradiation with 10 mg catalyst, 100 mL red seawater and 120 °C. Photocatalyst was stable for 3 cycles.	132
Water/oil microemulsion method				
Ag/AgBr/rGO-Si	*p*-Nitrophenol (PNP)	Visible light, 75 W halogen lamp	With 1 wt% catalyst and 1 mmol PNP: 95% photo-reduction of PNP to *p*-aminophenol after 20 min. 93% photoreduction of PNP to paracetamol after 8 min with 1 mmol acetic anhydride. 92% photoreduction reached after 3 cycles.	133
Ultra-sonication exfoliation method				
Ag-$FeCo_2O_4$/RGO	Rhodamine B (RhB)[d] benzimidazole	Solar light[b]	86% RhB degradation rate after 120 min. 54.46% benzimidazole degradation rate after 140 min.	134
g-C_3N_4	Rhodamine B (RhB)[d]	Direct sunlight[b], solar radiation on that particular day was 843 ± 2 W m^{-2}, and temperature was 26 °C.	59% RhB degradation rate after 60 min with 5 mg catalyst and 5 mg L^{-1}	111
High shear mechanical exfoliation method				
MXene (Ti_3C_2)	Methylene Blue (MB)[d]	Visible light, 300 W[c]	98% MB degradation rate by MXene-blender (MX-B) nanosheets within 60 min, 2 ppm dye and 1 mg catalyst.	135
Electrochemical exfoliation method – followed by hydrothermal treatment				
TiO_2	Methylene Blue (MB)[d]	UV, 8 W, characteristic wavelength = 254 nm	87% MB degradation rate after 20 min with 0.2 g L^{-1} catalyst and 5 ppm dye.	136
Thermal exfoliation (thermal etching) method				
g-C_3N_4	Rhodamine B (RhB)[d]	Direct sunlight[b], solar radiation on that particular day was 843 ± 2 W m^{-2}, and temperature was 26 °C.	86% RhB degradation rate after 60 min with 5 mg catalyst and 5 mg L^{-1} 0.4% photocatalytic activity lost after 4 cycles	111

[a] Red sea water sample containing: 386 ppm Ca, 14 310 ppm Na, 742 ppm Mg, 210 ppm K, 22 219 ppm Cl, 146 ppm HCO_3, 3115 ppm SO_4, 15 ppm NO_3, HPC > 6500 CFU per mL, 42 840 ppm TDS, 1320 ppm Total hardness at pH = 8.2. [b] Direct sunlight irradiation is known to fluctuate with time, in some cases these sources do not specify time, date, or position. [c] Unspecified light source – spectra unknown. [d] Organic dyes are known to have a sensitisation effect, potentially modifying the light adsorption spectra of a photocatalyst and affecting the apparent degradation.[137–139] [e] [sic] Methyl Orange.

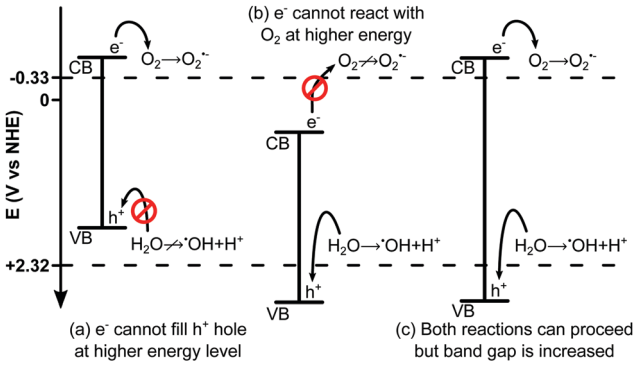

Fig. 6 Schematic illustration of redox potential for $^{\bullet}OH$ and $O_2^{\bullet-}$ showing (a) a semiconductor with sufficiently negative CB to allow $O_2 + e^-$, but VB too negative to allow $H_2O + h^+$ as H_2O cannot donate an electron to fill the more negative hole in the VB of the semiconductor. (b) A semiconductor with sufficiently positive VB such that H_2O may donate an electron to fill the hole, however the CB is too positive meaning O_2 cannot accept e^-. (c) A semiconductor with both a sufficiently negative CB, and a sufficiently positive VB. This semiconductor would be capable of facilitating both reactions but has an increased band gap, limiting its solar spectrum adsorption range. Heterojunctions (Fig. 7) can be used to reduce this band gap whilst maintaining the redox potentials. Figure is for illustrative purposes only and is not drawn to scale.

The irony of photocatalysis is that generally speaking it is preferable to have a small band gap to enhance the range of useful light irradiation, but a large band gap to enhance the creation of redox couples. By using two semiconductor materials in a heterojunction photocatalyst the redox potential of a photocatalyst can be increased without increasing the band gap.[152]

Fig. 7 gives a brief overview of the heterojunction schemes that are applicable to photocatalysis. The S-scheme (direct Z-scheme) is the most appropriate heterojunction for photocatalysis.[140] Type II heterojunctions do work but are inferior

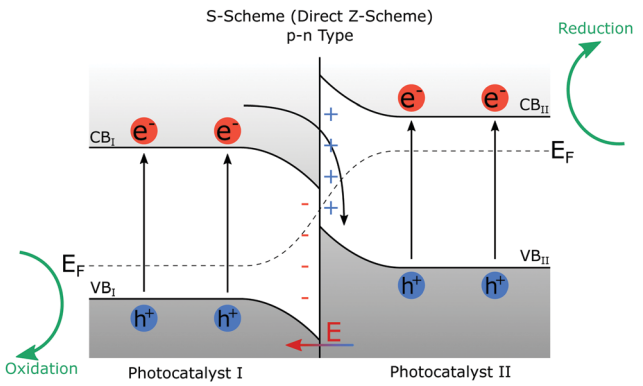

Fig. 7 Schematic diagram of a p–n type S-scheme heterojunction. E_F represents the Fermi level of the two photocatalysts and is seen to bend at the interface.[151] VB and CB are valence and conduction bands. Both photocatalyst I and photocatalyst II undergo photoexcitation, creating electron-hole pairs. Electrons in CB_I and holes in VB_{II} combine leaving strong redox potential electron-hole pairs in CB_{II} and VB_I. The redox potential of the heterojunction photocatalyst is greater than either of the catalysts individually, and the band gaps have not been increased to achieve this.

to the S-scheme due to the increased charge recombination and narrowed band gap leading to reduced redox potential, and minimised redox couple generation. In some instances,[153] this can lead to the absence of $^{\bullet}OH$, leaving only the weaker oxidising $^{\bullet}O_2^-$. S-Scheme heterojunctions can be p–n, n–p, n–n, or p–p type[151] where p (positive) and n (negative) refer to the charge on the two photocatalysts composing the heterojunction.

In the S-scheme, also known as the direct Z-scheme, heterojunctions of both photocatalyst I (PCI) and photocatalyst II (PCII) can undergo photoexcitation to create electron-hole pairs. The excited electrons from PCI combine with the holes of PCII leaving an electron-hole pair in which the electrons are in the conduction band of PCII (CBII) and the holes in the valence band of PCI (VBI) making it harder for them to recombine. This also allows the resulting CB and VB (and thus the redox potential) to be higher than that of Type II heterojunction in which CBI and VBII define the redox potential.[140]

4.2 Active sites

For 2D TMD nanomaterials, active sites occur mainly on the edge planes, leaving the basal planes mostly inert.[154,155] It has also been reported that GO is edge plane active[156] due to electron transfer mechanics at the edges, and that graphene (although not photocatalytically active on its own) has an electrochemically inert basal plane.[157] Other photocatalysts such as g-C_3N_4 have active sites on both the basal and edge planes.[145] Photocatalytic active sites require two things; (1) capability to accept charge carriers, (2) adsorption of the reactant molecule.[143] (1) Some 2D photocatalysts, such as g-C_3N_4, are unable to freely transfer electrons resulting in charge trapping. In g-C_3N_4 the bridged N1 atom (Fig. 8) prevents the transfer of charges between structural units.[145] This can result in charge recombination if there are no reactant molecules adsorbed on that structural unit. (2) For other 2D photocatalysts such as MoS_2 molecules are unable to be adsorbed onto the basal plane but are readily adsorbed to appropriate edge structures.[158]

The lack of active sites on the basal plane of most 2D photocatalysts can be addressed by a number of techniques. For example g-C_3N_4 has been shown to benefit from heteroatom doping creating defects in the basal plane where reactants can be adsorbed and which can also reduce charge trapping by the bridged N1 atom. Creating defects in g-C_3N_4 can also lead to nitrogen vacancies which can act as sites for charge recombination, decreasing the photocatalytic activity.[145]

5 Synthesis & morphology

Each technique used to synthesise nanosheets comes with its own trade-offs. For synthesis, high yields must be balanced with suitable nanosheet quality and morphology, as this has a significant effect on material performance. Large scale production should be developed with this in mind. The benefits of atomically thin PCs are well known,[12] but what is less understood is how the introduction of defects to the structure of PCs

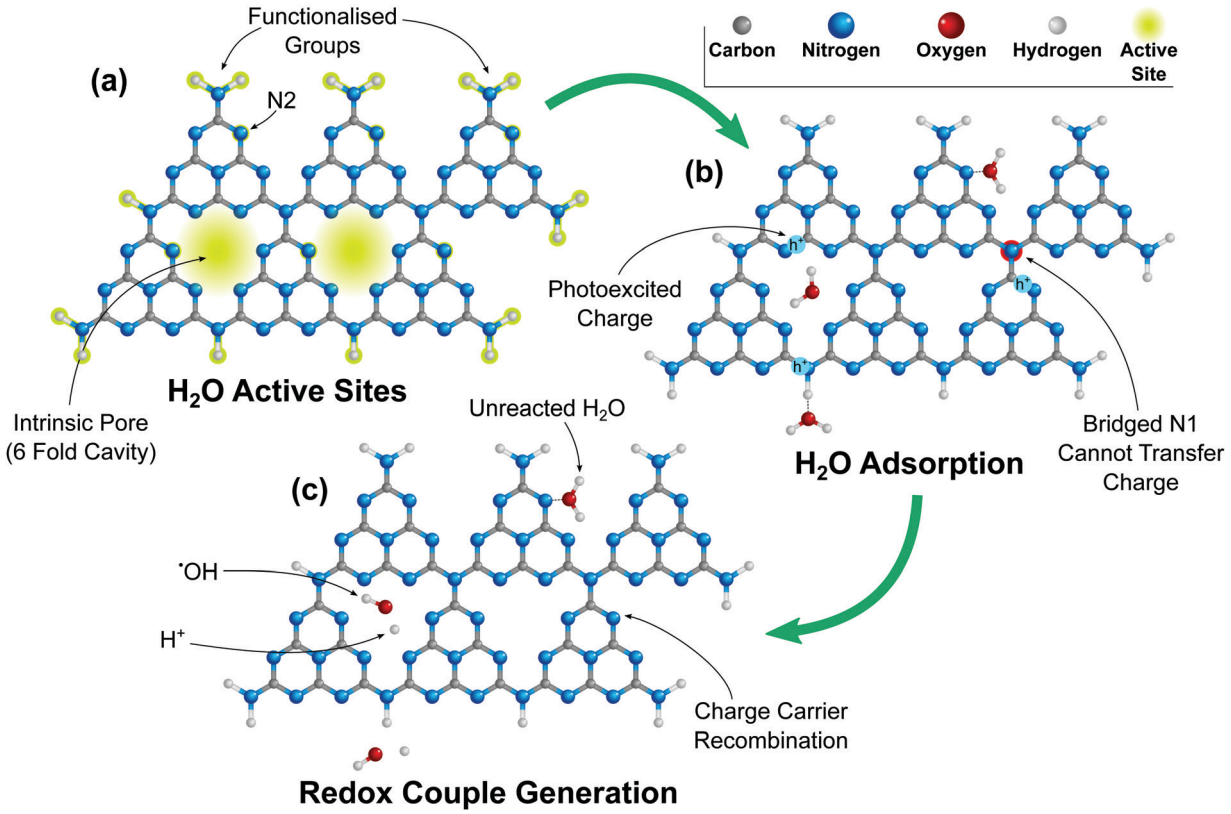

Fig. 8 Schematic diagram of g-C_3N_4 (tri-s-triazine (heptazine)) showing (a) H_2O adsorption sites, highlighted in yellow (b) H_2O adsorption onto g-C_3N_4 active sites, and electron trapping due to the bridged N1 preventing electron transfer between structural elements.[145] (c) Subsequent dissociation of H_2O into $^{\bullet}OH/O^+$ redox couple where sufficient charge carriers are available.

can increase the photo-activity of nanosheets.[159] Among these defects; pores, vacancies, pits and distortions can all act to impact the viability of the photocatalyst. Defects can be introduced directly through the initial synthesis route or by post-processing stages such as annealing.[160–162] Crucially, both pristine nanosheets and defective nanosheets are required, and many papers fail to fully characterise their findings in this sense.[163] This leaves a gap in research for examining the synthesis of nanosheets for photocatalysis in a practical sense. Synthesis of nanosheets can be divided into two areas:

- **Top-down**, where nanosheets are extracted through the exfoliation of a natural or synthetic layered material.
- **Bottom-up**, where nanosheets are constructed from base molecules through chemical reactions.

Most methods of synthesis discussed in this section are top-down processes, as they are inherently scalable[164] and many are generally applicable to a wide variety of 2D materials (Table 2). Nanosheet synthesis through exfoliation of a precursor material is a primary top-down route, which can be achieved using a number of techniques illustrated in Fig. 9. Facile synthesis of pristine nanosheets would ultimately lower the cost of manufacture for composite-PCs and allow researchers and practitioners to streamline the production of their own advanced PCs. Take g-C_3N_4 as an example, with a straightforward synthesis route which can be realised through a number of different

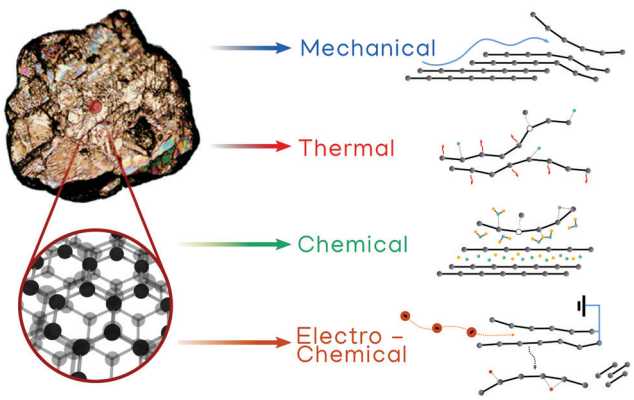

Fig. 9 Schematic representation of the different exfoliation techniques discussed in this review: liquid-phase "mechanical", thermal, chemical and electro-chemical exfoliation.

methods,[165] has led to many papers discussing its excellent photocatalytic properties;[166] however, most use inherently unscalable production processes.[167] The use of appropriate techniques which can move synthesis of nanosheets away from the lab scale and into industry are essential in the long-term.

Importantly, there are many characteristics to consider with varying levels of importance depending on the end-use. Production rate, defects introduced to the nanosheets, power

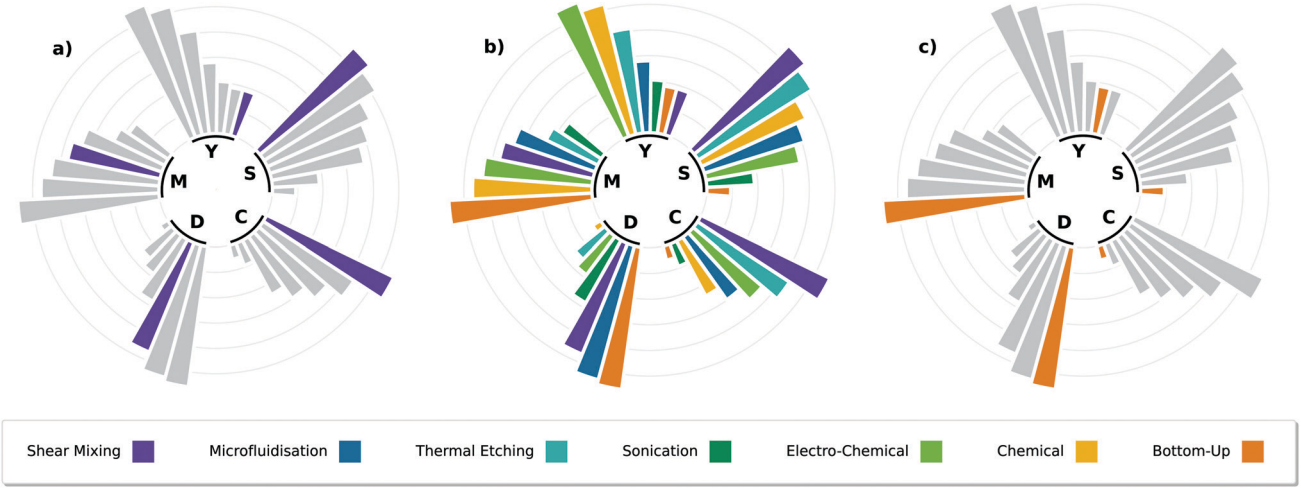

Fig. 10 Circular barplot of all the synthesis techniques discussed in this section, ranked according to the process parameters of scalability (S), yield (Y), morphology (M), defects (D) and cost (C), subplot (b). Subplot (a) isolates shear mixing, a technique which suffers almost exclusively from its poor yield (typ. ~ 1–10 wt%). Subplot (c) isolates bottom-up methods, in this case Chemical Vapour Deposition (CVD) has been used as an example. CVD can be used to grow different materials on substrates, and is currently the most widespread technique for fabricating pristine monolayered graphene on copper substrates.[170]

consumption, yield and morphology can be sensitive to the synthesis method and accompanying post-processing operations (*e.g.* centrifugation settings).[168] Therefore, a direct comparison of different synthesis routes is non-trivial. To accommodate this, each process subsection has been ranked against each other in Fig. 10 which separates the issue of production into five sub-topics, in the spirit of Raccichini's work,[169] scored out of a maximum of 3.

- **Scalability (S)**, the quality of a process that can be scaled up, through larger process volumes and concentration.
- **Yield (Y)**, the mass concentration of nanosheets with respect to the initial precursor concentration. Note that a process which is scalable can often be cost-effective even at a low yield through sheer volume.
- **Morphology (M)**, encompasses the shape and thickness of the final product. Products with low number of atomic layers scores highly.
- **Defects (D)**, takes into account the defects present in a material due to the method of production (e.g. basal plane vacancies). A low score indicates a defective nanosheet (which can be beneficial).
- **Cost (C)**, a low cost efficient system (by starting capital and running costs) scores highly in this examination.

5.1 Mechanical exfoliation in liquids

Mechanical exfoliation is the process of taking a layered precursor material composed of 2D nanosheets held together by weak van der Waals forces, and breaking it down into its constituent nanosheets through the application of an external mechanical force. Many of the techniques described here involve liquid-phase dispersion routes to exfoliation, and are termed Liquid-Phase Exfoliation (LPE) methods. LPE has been seen as a facile and scalable route to synthesis since soon after the discovery of graphene.[171] It typically requires additional post-processing steps to separate the synthesised nanosheets from the unexfoliated bulk material.

LPE processes disperse layered materials in an appropriate solvent, with the precursor predominantly in the form of microscale particles or flakes. The choice of solvent in suspensions is key, as the dispersion of the nanosheets must match the dispersion of the solvent in order for the solution to be stable and avoid re-aggregation of the sheets.[172] This can be achieved through traditional solvents (*e.g. N*-methyl-2-pyrrolidone, NMP), co-solvents, or the addition of surfactants in aqueous solutions that resist nanosheet restacking by steric or electrostatic repulsion.[168] Furthermore, an adequate choice of solvent can act to enhance exfoliation.[173] For example, the bio-compatible solvent cyrene has been shown to have the same dispersion characteristics as graphene, and methods using this combination are showing greatly improved exfoliation yields than previous attempts with other high-performance toxic solvents (*e.g.* NMP).[174]

Another aspect to these techniques is that they are generally applicable to all layered materials, and tend to produce defect-free nanosheets compared to other techniques, due to their being a mechanical route to exfoliation. Some defects can be introduced in the process; sonication produces localised regions of high shear rate through the rapid collapse of microbubbles during cavitation, which although exfoliating, can also begin to produce holes in the nanosheet lattice. Shear mixing also produces high localised shear rates, at a lower magnitude, exfoliating nanosheets without basal plane defects. Microfluidisation can achieve some of the largest shear rates ($>10^6$ s^{-1}) to effectively overcome van der Waals forces but suffers from a high power consumption to instigate turbulent flows in microscale channels. Hence, there can be a number of trade-offs to consider when selecting synthesis strategies for photocatalytic materials that are producible on a large scale.

In this review, we focus on three techniques that are commonly used to produce nanosheets through liquid exfoliation. A variety of other non-oxidising techniques can be found documented elsewhere.[168]

Sonication

Sonication has been the *de facto* process for creating nanosheets in the lab since its demonstration in 2008.[171] Its prominence is due to its simplicity, as it often uses readily available lab equipment; namely, bath sonicators and probe sonicators (Fig. 11). This equipment is typically used to homogenise mixtures, but exposing a bulk precursor to these environments for extended periods of time induces exfoliation of its constituent nanosheets.[175] The exfoliation of the precursor is caused by ultrasonic waves emanated by the sonicator, the mechanics of which were not fully understood until recently.[176] As sonication is a predominantly physical route to exfoliation, it works with a wide variety of layered materials.

Sonication suffers from difficulties surrounding scalability, as the rate of production does not scale well with increasing volume.[177] A peak in nanosheet production has been observed depending on concentration and volume used,[178–180] which is a difficulty for large scale production of nanosheets. Large sonicating probes are available industrially, but are prohibitively expensive, and can require the implementation of batch-type processes. Sonication can also cause defects within the exfoliated nanosheets, such as holes within the basal plane, but it is not clear yet whether this is to do with extended exposure to a high shear environment.[181,182]

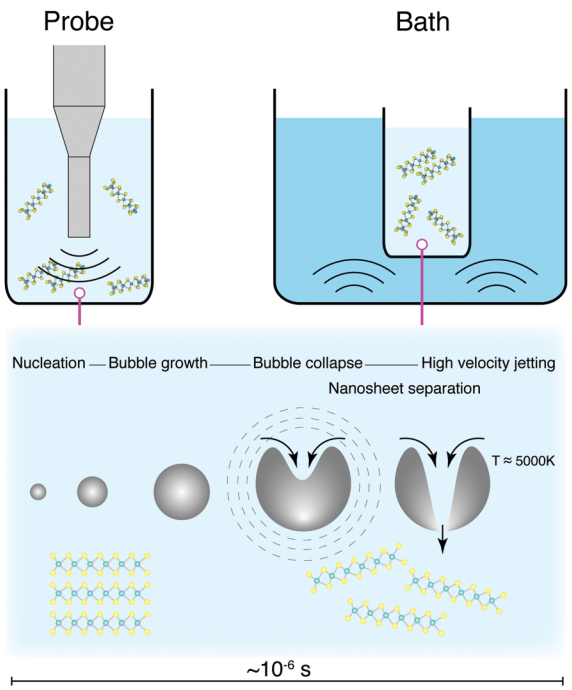

Fig. 11 Sonication-based synthesis typically involves either probe or bath techniques. Exfoliation of layered materials into nanosheets is achieved through the rapid growth and collapse of cavitation bubbles in the liquid dispersion.

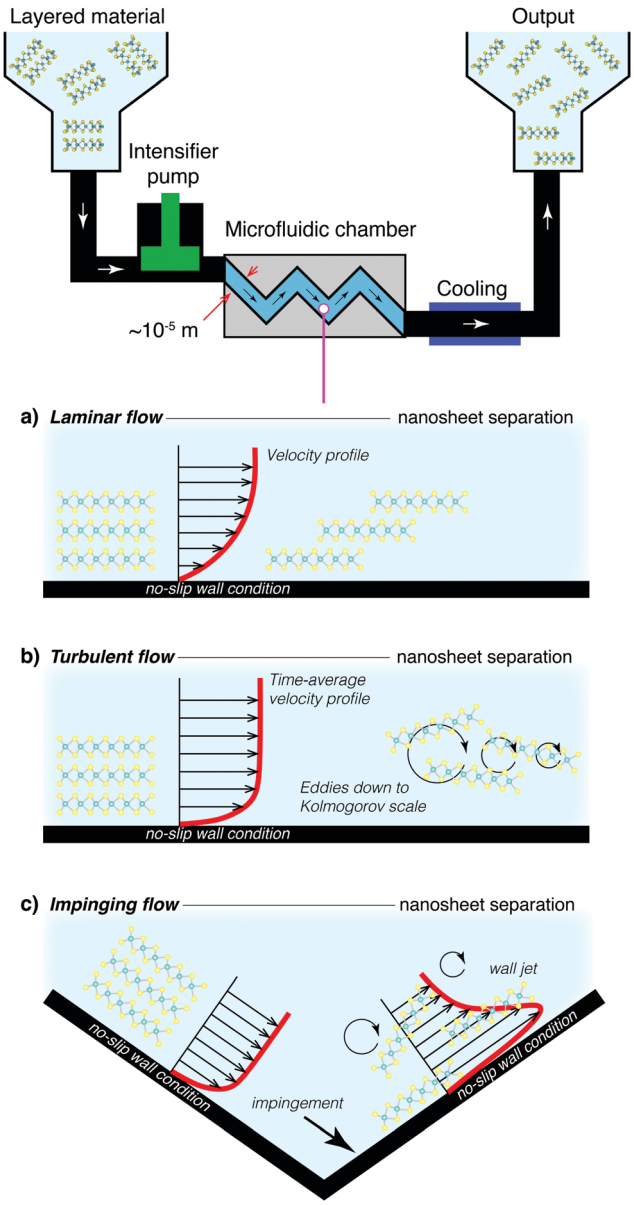

Fig. 12 Microfluidisation of nanosheets from layered materials. The synthesis mechanisms depend on the hydrodynamic regime and chamber configuration. Production of nanosheets can be achieved through (a) laminar or viscous shear exfoliation, (b) turbulent shear exfoliation and/or (c) localised flow impingement.

Microfluidisation

Microfluidisation for LPE is a relatively recent method, and was first demonstrated in 2017.[167,183] The process involves pumping a precursor/liquid mixture through a series of microfluidic channels, where the extreme shear forces within the channels (which include bends, tight turns, localised flow impingement and wall jets[184] that induce high shear stresses) exfoliates the precursor (Fig. 12). The equipment required for this type of method is relatively common, as similar machines are used in the pharmaceutical industry for homogenising mixtures. The key difference is that exfoliation requires a longer exposure to

the shear within microfluidic devices, which in practical terms means more passes through the same reactor or a longer reactor.

The method has demonstrated complete conversion of graphite into micro/nano-platelets with thicknesses up to 70–200 nm.[167] However, the yield of few-layer graphene with average number of atomic layers less than 10 has been found to be typical of other high-performance shear exfoliation techniques at around 3%.[183] Other critical examinations of this methodology are required to address some of the practicalities for scale-up.

The microscale channels are often similar dimensions to the particle precursor (~10–100 μm), and can agglomerate within the small channels leading to clogging. Blockages in these systems can clearly be laborious to halt and clean. High shear stresses within the reactor result in viscous heating and large increases in temperature within the microfluidic device. Both high pumping power and cooling contribute to the total power required for operation when considering process efficiency. These items may be seen as minor or secondary issues in low volume laboratory or pilot synthesis. Extending the approach to high-throughput operation and varied starting materials, however, and batch failures, product variability, process down-time and energy use become important factors for material quality and cost.

Shear mixing

Shear mixing concerns the set of LPE processes that focus on applying a shear force to the liquid–precursor mixture, above a critical shear rate for exfoliation, such as $\dot{\gamma} > 1 \times 10^4\ s^{-1}$ for graphene and $\dot{\gamma} > 3 \times 10^4\ s^{-1}$ for semi-conductors MoS_2 and WS_2.[164,185] This kind of setup is inherently scalable and much of the technology is already widely used in large scale batch mixers, or even in small scale kitchen blenders.[177] These systems are however not optimised for nanosheet synthesis, and a purpose built system could reduce energy consumption and ensure a more homogeneous distribution of shearing forces within the mixture. Current high shear mixing designs focus on localised shear using batch homogenisers,[164] such as the rotor-stator arrangment illustrated in Fig. 13. This will obviously require further process optimisation, either through targeted computational fluid dynamics studies[186] or through repeated design iterations. Nonetheless, the groundwork is there for a successful process which would work on multiple materials and have minimal impact on quality or defects.

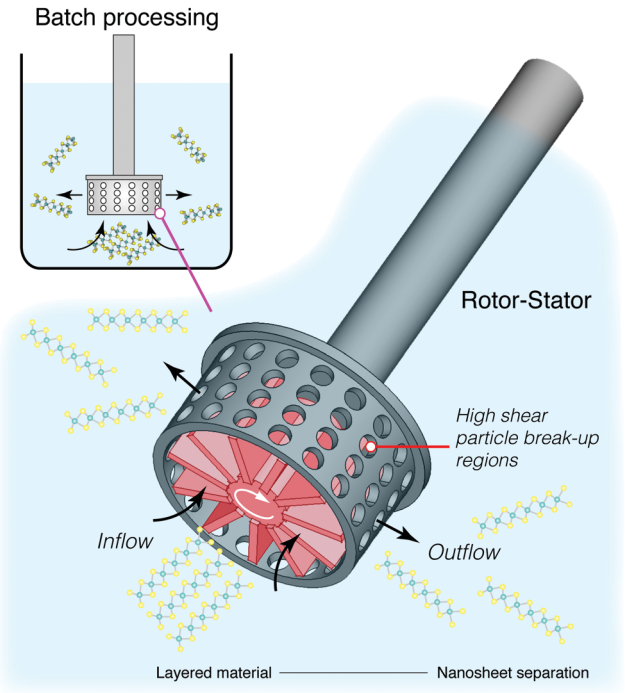

Fig. 13 Synthesis of nanosheets using high shear mixing. Exfoliation and precursor particle break-up predominantly occur in the rotor (red) and stator region of these devices where collisions and the largest shear stresses in the batch volume exist.

5.2 Thermal exfoliation

Thermal exfoliation consists of exposing a precursor, or a suspended precursor mixture to high temperatures (≈500 °C depending on the material). The variations on this method are illustrated in Fig. 14 for the synthesis of g-C_3N_4 nanosheets. The first example exposes a bulk material containing an intercalant to high temperatures which lead to the decomposition of layers in the lattice through the release of gases. This also promotes the formation of pores in the basal plane that can increase surface area for photocatalysis.[187] The second example exposes a bulk material to high temperatures in air, driving layer-by-layer oxidation, together with layer splitting and large volumes of gaseous product release.[188] This exfoliates and thins layered precursors, as well as leading to particle fragmentation and pore formation. For both synthesis routes, the precursor is usually dry, and can be exposed to an inert environment in some cases to avoid doping the nanosheets with oxygen. When applied to 2D materials, the process shown in Fig. 14b) is sometimes labeled thermal etching, which is indicative of a much more targeted application of heat; though this is rarely the case in practical use and is more aptly termed thermal annealing.

This basic methodology is widely known to create defective nanosheets with vacancies (see Fig. 15), inclusions and even large holes.[189] Depending on the purpose, this type of synthesis can have beneficial effects on the performance of the photocatalyst.[111] This approach is most prominently used in conjunction with g-C_3N_4, where it has been proven as a highly effective photocatalyst.[190] In contrast, thermal annealing of graphite produces highly defective graphene, which does not perform well as a charge carrier, but can be used as a photocatalyst in its own right.

A system like this is inherently scalable, and may provide a reasonable yield, though the quality and defectiveness of the nanosheets produced is not always adequate. Although these defects are easy to introduce, it is significantly challenging to remedy with post-processing. Therein, this method of synthesis is applicable to a few specific cases, and should be treated as a purpose-dependant method of synthesis.

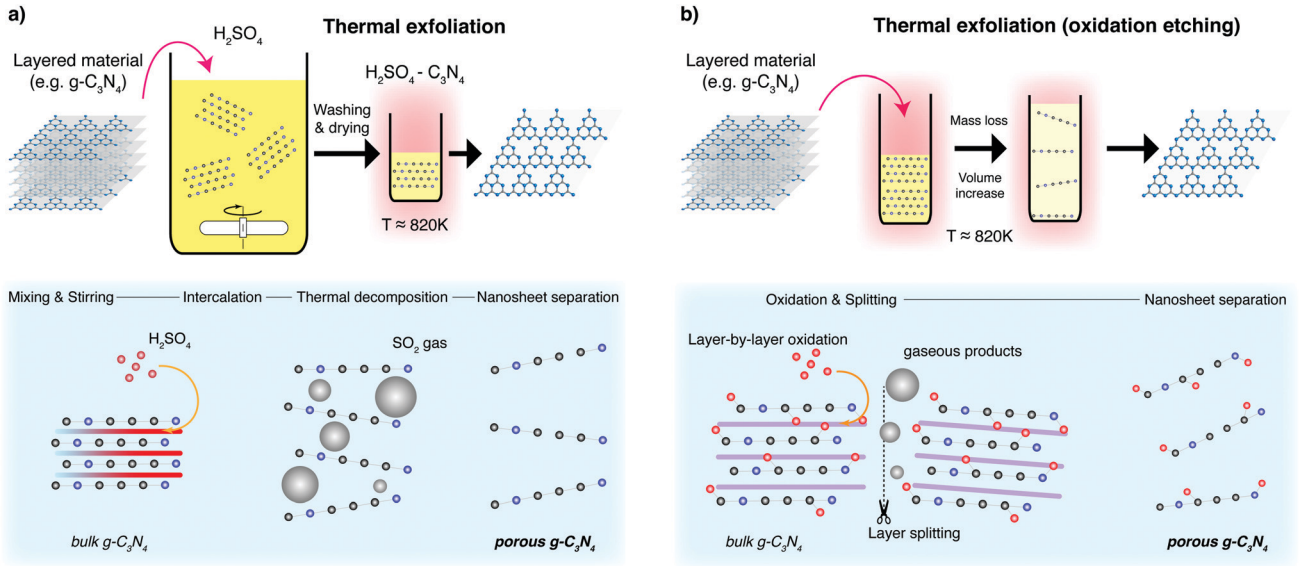

Fig. 14 Synthesis of nanosheets using thermal exfoliation can be achieved through a variation of thermal treatment approaches. (a) Intercalation of H_2SO_4 between layers leads to the formation of gas bubbles during the heating and thermal decomposition step, leading to the separation of nanosheets. (b) Thermal decomposition in air leads to layer-by-layer oxidation and layer splitting processes with gaseous products released. Fragmentation of nanosheets, together with the formation of pores and defects, also occur using these approaches.

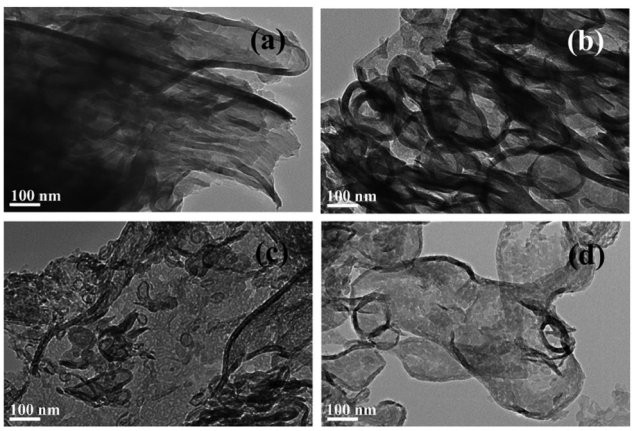

Fig. 15 TEM images of bulk g-C_3N_4 (a), alongside porous g-C_3N_4 exfoliated at 450 °C (b), 500 °C (c), 550 °C (d). The heat decomposes certain areas of the nanosheets, leaving the resultant sheets ranging from slightly exfoliated and porous to fully exfoliated and with large holes. Reproduced with permission from ref. 188. Copyright 2015 Elsevier B.V.

5.3 Intercalation

Non-mechanical routes to exfoliation typically involve chemically intercalating foreign molecules or atoms in between the layers of the crystal to exfoliate the precursor directly, or to assist mechanical exfoliation. These routes often oxidise, to an even higher degree than that of thermal exfoliation. Non-oxidising routes to exfoliation can be preferred to oxidising routes, as the introduction of new defects is much easier than the removal of pre-exsisting defects. Intercalation is oxidising, as it is unavoidable that some of the intercalated ions adhere to the nanosheets after exfoliation. Intercalation alone can also leave small parts of the precursor material untouched, and therefore it is usually complimented in the literature with some form of mechanical exfoliation to assist the decomposition of these leftover unexfoliated materials.

Electrochemical exfoliation

Many layered materials are conductive or semi-conductive, and this property permits some 2D nanosheets to be synthesized through electrochemical interactions (Fig. 16). In practice, these methods resemble electrolytic reactions, with the cathode being replaced with a raw precursor ore (such as graphite); when a voltage is applied across the electrodes, charged ions permeate the precursor and break it apart. For highly conductive materials such as graphene, this method has been proven to be a facile method to create GO.[191] Certain photocatalytic nanosheets can also be fabricated in a similar way,[192] though conductance does limit the range of materials which can be synthesised. This method of synthesis has rarely been explored for manufacturing 2D-PCs, but not because of the conductive threshold. Typically, there exists more proven routes to synthesis (such as sonication or thermal annealing) and therefore the potential of electrochemical processes has not yet been fully explored, even though a variety of PCs such as MoS_2, WS2 and g-C_3N_4 have been synthesised.[193] The production rate is favourable in comparison to other methods, and the level of oxidation can be tailored, in some instances, by adjusting the applied voltage difference between electrodes.

As highlighted, defective PCs can be advantageous, therein, this technique does seem to offer a scalable route to production for many suitable photocatalytic materials. However, many of these bulk materials range in conductivity, indicating that some of the potential difference applied to the electrodes will

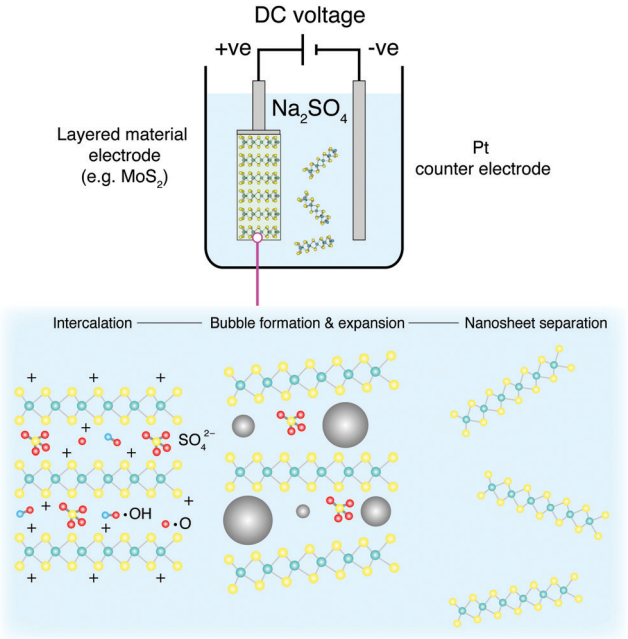

Fig. 16 Synthesis of nanosheets using electrochemical exfoliation. Intercalation of radicals and anions between layers leads to the formation of gas bubbles and separation of nanosheets. Oxidation of nanosheets can occur depending on the applied voltage, electrode configuration and other experimental conditions.

be spent overcoming the internal resistance of such a system. This can be mitigated by the use of a conducting additive such as Li^+, but this complicates the process.[192] Furthermore, the product is not strictly composed of mono- or few-layers, but can contain stacked unexfoliated precursor particles which break off and subsequently cannot be exfoliated further due to their distance to the electrodes.

Chemical exfoliation

Chemical exfoliation requires enough time for a chemical solution to intercalate between layers before applying a chemical reactant to break apart the van der Waals forces, separating the layers (Fig. 17). A number of PCs, including g-C_3N_4, can be manufactured by exposure to concentrated sulfuric acid and a subsequent exothermic reaction with water.[194] This kind of process is far more toxic and laborious than other more simple methods (often taking at least 4–5 hours), and ends up producing much more defective nanosheets, improving the photocatalytic properties of synthesised g-C_3N_4 further than those produced by thermal exfoliation.[195]

When applied to graphite, this methodology is known as the modified Hummers' method, and produces highly functionalised GO.[196] The sheets produced are morphologically well-formed large mono- and few-layers, with some pores induced through the exothermic reaction. These sheets require intensive post-processing to form reduced-GO (rGO) nanosheets with a reduced defect quantity. By themselves, functionalised GO sheets can perform as PCs, but do not perform well as charge carriers.[197]

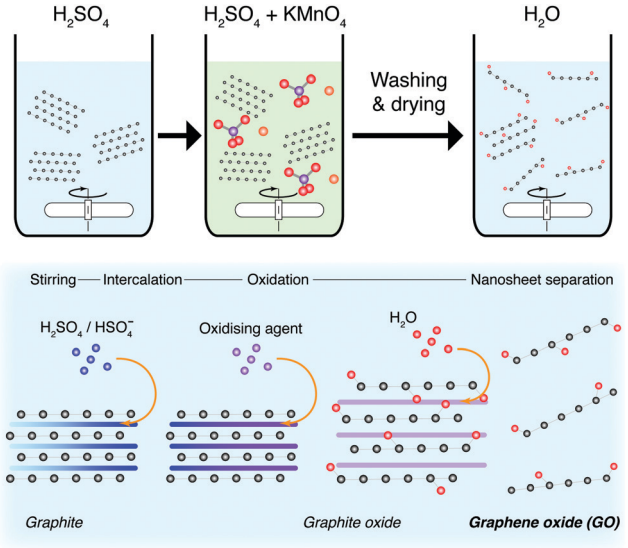

Fig. 17 Synthesis of graphene oxide nanosheets. Chemical exfoliation is typically achieved using a modified Hummers' method. Graphite is oxidised to form graphite oxide, followed by dispersion and separation of GO nanosheets in water.

5.4 Composites

Photocatalytic composites account for approximately one third of the total published research online (when comparing "synthesis photocat" to "synthesis photocat composite" on the Web of Knowledge). Of which, half mention the use of TiO_2 while just under a quarter include graphene. Both of these materials are excellent supporting materials for visible light active PCs, but do not perform well on their own.

Combining charge carriers and dedicated PCs as a composite material provides a route for electron-hole pairs to separate efficiently and react with the surrounding water. Prefabricated nanosheets mixed in solution are essential to all of these methods. In that regard, the methods discussed here are approaches that can further the viability of composites in photocatalysis and enable the intrinsic advantages of nanosheet PCs to be fully exploited.

Hydro/solvothermal synthesis

In terms of synthesising composite-PCs, just over half of the total studies into synthesising composite photocatalysts included the terms "hydrothermal" or "solvothermal". The prevalence of hydro/solvothermal synthesis is due to its simplicity and the variety of composites that can be produced (see Table 2). It typically only requires the mixing of disparate materials in solution, then under the application of an external force (heat and pressure), the constituents can be brought close enough to bind or react together (Fig. 18). Hydrothermal and solvothermal differ only in the reaction medium be it aqueous (hydro-) or solvent (solvo-) based. The conditions required for the process are typically only achievable in an autoclave, though not all hydro/solvothermal processes require extreme temperatures and pressures. Hydro/Solvothermal synthesis can also be

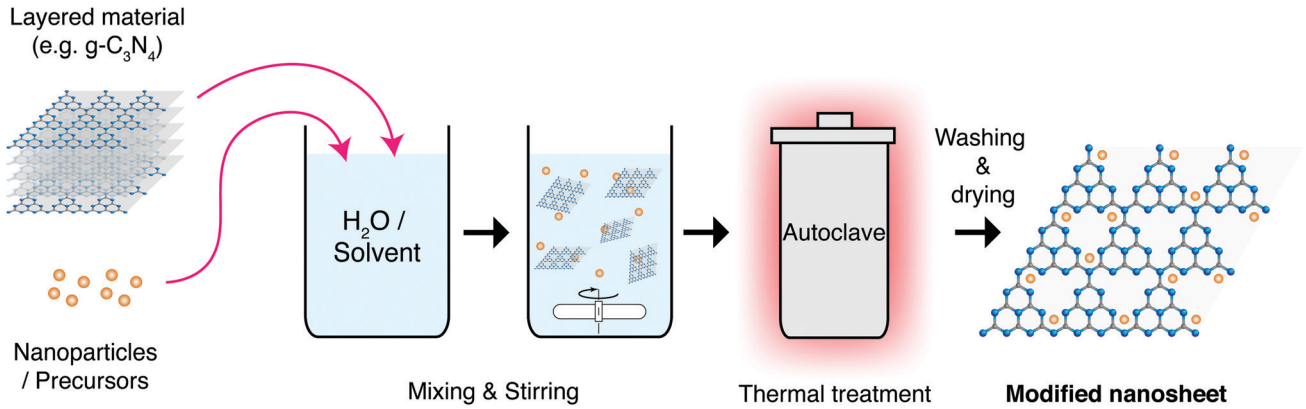

Fig. 18 Schematic representation of the solvo- or hydrothermal synthesis process for producing nanosheets and nanocomposites.

used to tune the nanostructure of various nanomaterials and increase their photocatalytic activity.[57]

Hydro/Solvothermal synthesis has been used with great success to apply nanomaterial coatings to nanosheets. Graphene is one of the most prominent materials here, with many inorganic nanocrystals being successfully deposited on its surface, irrespective of its oxidised state. These materials include Metal Oxides, Nitrides and Chalcogenides, among others.[198] These composites can take a variety of shapes and forms as shown in the example in Fig. 19 for rGO coated TiO_2 nanoparticles.[199]

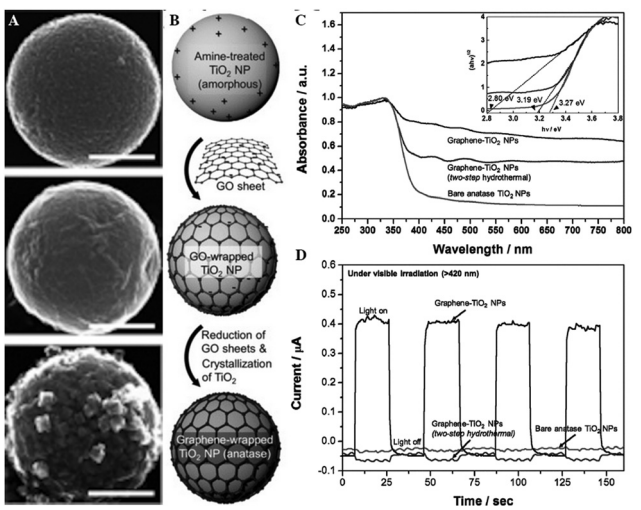

Fig. 19 An example of a hydrothermal route to composite synthesis, with corresponding SEM images (A) and photocatalytic activity. (B) shows a schematic representation of the route, where rGO coated TiO_2 nanoparticles (NPs) were created through a combination of electrostatic interactions and in-solution mixing, followed by simultaneous hydrothermal reduction of the GO into rGO and crystallisation of the initially amorphous TiO_2 NPs (graphene-TiO_2 NPs). These NPs were compared to separately crystallised TiO_2 followed by the same electrostatic-assembly and hydrothermal reduction (two-step hydrothermal), and bare anatase NPs, in terms of their photocatalytic (C) and photoelectric activity (D). The scale bars shown in (A) represent 200 nm. Figure adapted from Lee *et al.*[199] Reproduced with permission from ref. 199. Copyright 2012 John Wiley & Sons Inc.

Templated growth/assembly

2D nanomaterials can also be used as templates on which a variety of exotic structures can be formed. Porous g-C_3N_4 nanosheets created through thermal exfoliation can be coated in a secondary co-catalyst or charge carrier nanomaterial to greatly improve its photocatalytic activity. These nanostructures provide abundant surface area and improved light scattering, with improved mass transfer of pollutants through the structure.

The most commmonly templated nanomaterial is again graphene, however these processes are more sensitive to oxidised graphene, meaning that epitaxial growth of nanostructures has only been demonstrated on pristine graphene sheets, manufactured out of solution.[166] Therefore, full epitaxial growth of 2D/2D heterostructures is currently reserved for the lab scale and unsuitable for the large scale synthesis required for photocatalysis. A variety of 2D nanosheets have since been grown on in-solution graphene, including the main classes of photocatalysts discussed here.[200] These nanostructures often have much better adhesion to the templated material, demonstrating a greatly enhanced photocatalytic activity. Templated assembly (self-assembly) defines the materials to be fully formed before combination. These assembly techniques (much like hydro/solvothermal methods) often require some external energy or take advantage of the electrostatic interactions between materials.[197]

Other synthesis routes

Though other routes to synthesis have been explored for composites which deposit atomically thin layers of material (*e.g.* chemical vapour deposition),[201] their suitability for the wide range of photocatalytic water treatment applications is limited. Composite synthesis for photocatalysis should be as scalable an approach as possible, due to the amount of material required for industrialised water treatment. Additionally, the variety of approaches, from immobilised to mobilised, tends to favour the use of general solution processing methods. Thus, simple one-pot methods and self-assembling techniques will mainly be preferred due to their robust and scalable nature.

6 Treatment & reuse

Much like synthesis can affect morphology, practicality plays a role in the implementation of photocatalytic materials for real-world water treatment applications. With this in mind, the groundwork of specific treatment and reuse cases can be broken down into three parts:

- The treatment stage, or the application of a photocatalyst to water purification.
- The separation or filtration of the photocatalyst from the water.
- The reapplication and re-usability of the photocatalyst after the first use.

These factors can be tightly interlinked as shown in the schematic of Fig. 20 for different approaches. Each individual photocatalyst then brings its own pros and cons. Some obvious ones include material activity, ease of synthesis and processing. Other features such as the PCs tendency to aggregate to other particles, or the average size of the photocatalyst, are less obvious. 2D materials are inherently difficult to separate from treated water, as any technique utilising the photocatalyst in suspension must then apply suitable filtration to remove the catalyst from the water. This adds resistance to the flow, and additional treatment stages and complexities, ultimately increasing the running costs to the point where it is unsustainable.[202] Therefore, the larger the photocatalyst, the more trivial the separation and reuse; but any decrease in the surface area of the photocatalyst in contact with the water has a detrimental effect on the photocatalytic activity, and *vice versa*. This interdependence marks most trade-offs and choices for the application of PCs in water treatment, and is illustrated in Fig. 20.

Generally it would appear that the reuse of PCs is effective with little loss in efficacy with each reuse cycle. Panthi *et al.*[203] show two studies testing the reuse of PCs, neither of which show a substantial loss in overall treatment efficiency, or treatment time. Xu *et al.*[204] also show two studies with similar results. PCs can be applied in many ways, so long as they make contact with the water, are irradiated with light with energy greater than or equal to their band gap (see Fig. 3 and 4), and have a suitable band gap to create redox potentials (see Fig. 6). These factors should ideally be maximised but due to practical limitations, this cannot always be the case. Treatment methods are hence split into two groups depending on how the photocatalyst is allowed to contact the water, *e.g.* whether it has been *immobilised* on a substrate or whether it is *suspended* within the fluid (or allowed to mix liberally).[205]

6.1 Immobilised

Immobilised PC are at first glance the more practical in terms of large scale implementation, with systems trading efficacy (due to reduced active sites in contact with the fluid) for

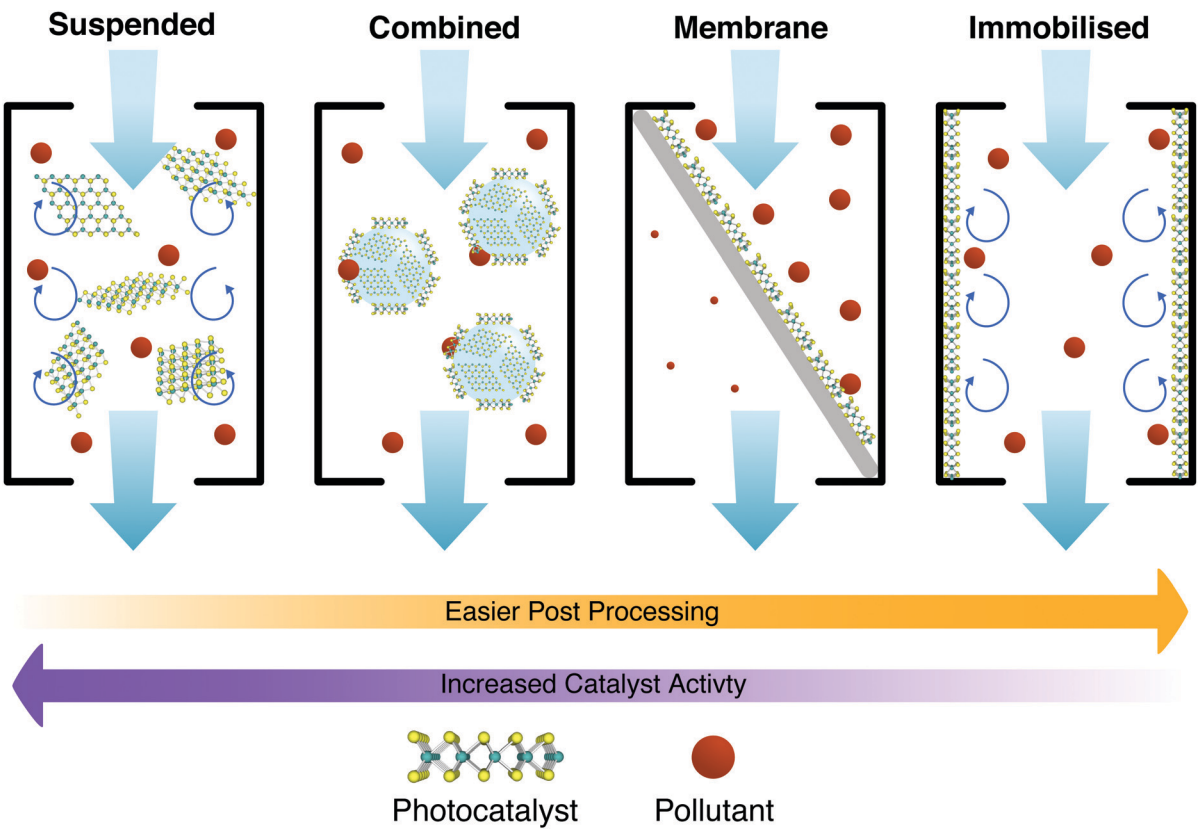

Fig. 20 Schematic illustrating the different levels of immobilisation discussed throughout the text (suspended, combined, membrane, and immobilised). From left to right, the challenges in removing 2D photocatalysts from the treated water decrease, however, the catalyst activity also tends to decrease.

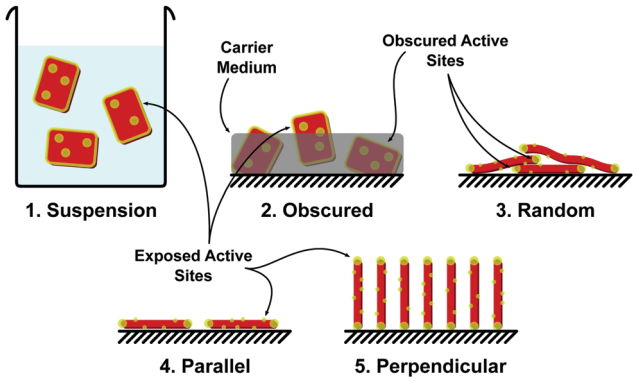

Fig. 21 Schematic diagram of various 2D photocatalyst alignments showing the active sites that they expose: (1) photocatalyst in suspension exposes all active sites, (2) photocatalyst in a carrier medium obscures active sites within the medium, (3) randomly deposited photocatalysts (*e.g. via* dip coating) layer over each other obscuring active sites, (4) alignment controlled deposition (*e.g.* Langmuir–Blodgett film deposition) resulting in photocatalysts parallel to the substrate, exposing basal plane active sites on the free side of the film. This type of deposition can be difficult to achieve with a single layer of photocatalyst and will usually have multiple layers, obscuring the active sites of all but the surface layer. 2D photocatalysts must be basal plane active (*e.g.* heteroatom doped g-C_3N_4). (5) Alignment controlled deposition resulting in photocatalyst deposition normal to the substrate surface (*e.g.* high voltage electrophoretic deposition). This exposes much of the active edge site but may obscure some basal plane active sites.

simplified operating procedures, negating the requirement for a recovery stage. In terms of cost scaling, these methods increase in efficiency when scaled.[206]

Limited active site availability has been discussed earlier in this review with methods such as heteroatom doping to increase the number of active sites on a 2D photocatalyst introduced. It is also important when considering immobilised photocatalysts that the exposure of active sites be considered. Many immobilisation techniques such as dip coating, immobilisation within a carrier medium, inclusion in a membrane precursor dope, can act to block active sites. Methods to increase the active sites on the basal plane of a material are still of importance, especially when particles are aligned parallel to the deposition surface. When considering immobilised photocatalysts at the 2D material scale, a number of configurations may be possible, including: (1) suspension (non-immobilised), (2) obscured (in a carrier or membrane dope), (3) randomly immobilised, (4) parallel immobilisation, and/or (5) perpendicular immobilisation (Fig. 21).

6.1.1 Photocatalytic coatings (PCCs)

PCCs have gained significant attention for NOx abatement in urban environments, though there is debate over their effectiveness (sources vary wildly, but it is likely $<2\%$ reduction).[207] The coatings used vary in the use of suspension medium, porosity, and roughness that the actual effectiveness of the PC is obscured. What does stay consistent is the choice of commercial P25-degussa, a now lower performing photocatalyst in a rapidly evolving field. In the sphere of water treatment, PCCs represent a significant section of the research area, with preliminary studies showing that such techniques are realistic and somewhat effective.[208–210] The efficacy of this technique is highly dependant on reactor design, as maximising the mass transfer at the boundary layer is essential for the proper functioning,[211,212] the mathematics of which are described in a comment by Turchi and Ollis.[213] Therein, internal coated structures or extending contact surfaces are essential for maximising the potential mass transfer over the photocatalyst. A benefit of these systems is that they are suitable for continuous and semi-batch processes.

Issues with PCCs stem from their highly reactive nature, which in turn make them sensitive to environmental conditions in terms of mass loss and colour change.[214] Though PCCs remain active and can slightly increase in activity throughout their life as the coating is degraded exposing new active sites,[215] the effect of PCCs leaching nanomaterial into water supplies at a large scale would impact water quality downstream and have unknown health effects.[216] At industrial scale, PCCs become difficult to implement as the space required for effective throughput scales poorly compared to suspended methods.

As well as the previously discussed PCCs which immobilise the PC in a carrier medium, such as a paint, PCs can also be coated directly onto a surface. Bayat *et al.*[217] immobilised MoS_2 nanosheets on Fluorine-doped Tin Oxide (FTO) slides for hydrogen evolution reaction. Using FTO negated the need for a binder material, reducing the potential for mass loss and coating degradation. This approach has the same scalability concerns as previously mentioned and is not applicable in urban spaces such as for NOx remediation.

6.1.2 Photocatalytic membrane reactors (PMRs)

PMRs in this case refer to those which immobilise PC with a membrane in order to increase the mass transfer over the immobilised photocatalyst. This can be by inclusion in the membrane dope to form mixed matrix membranes (MMM),[218,219] on a membrane surface,[220–223] or the membrane can be fabricated directly from PC material[56,224,225] (less common). This is important to note as suspended photocatalytic slurry reactors with a membrane based PC recovery stage are sometimes dubbed slurry-PMRs.[226] PMRs have been applied at medium to large scales throughout the past decade, with early tests determining that increasing the efficiency of such systems would be essential to their long-term adoption.[227] This could be realised by improving the quality of the photocatalyst; Increasing the surface area exposed to water, by changing the reactor shape/design; and/or improving the suspension medium/mesh. Indeed, these early tests saw a 50% improvement simply by switching the suspension medium.

Zheng *et al.*[228] provides an exhaustive list of the myriad of factors which can influence their performance, and notes that they have been used with success to treat campus sewage, pharmaceutical waste and micro pollutants, among others. PMRs can also be readily deployed in many ways as a continuous, semi-batch or batch process. One of the main challenges to this technique is the fouling of the membranes, which can be abated to some extent *via* good reactor design,[229] though

efficiency dictates that reactors are designed such that the flow passes through and not along the photocatalytic membrane for optimal performance (aptly named ''flow-through'' membranes).[230] Hence, PMRs behave like enchanced PCCs, yet are on the whole more difficult to construct and bring about issues with membrane fouling.

6.2 Suspended

Suspending PCs in water provides the highest quantity of active sites to be exposed at all times. The downsides of this method include turbidity in the liquid, caused by pollutants or PCs, and the requirement for an additional processing step to remove PCs from the effluent. Suspended applications usually require batch processes which can be less advantageous than continuous flow processes.

6.2.1 Magnetically seperable PCs

Magnetic Nano-PCs (MNPCs) have been experimented with for some time,[231,232] and typically involve the aggregation of a photocatalytically active material onto a larger magnetic particle. This allows for facile separation of the MNPCs while maintaining good contact area with the water. Improved material recovery alone will lower costs, and allow for more exotic constituents (such as noble metals) in a photocatalytic composite for even greater efficiency; however, increasing the life-span also introduces concerns about the photo-stability and photo-corrosion properties of the specific MNPC.[233] The design of such systems have been proposed,[234] and have very recently been applied at scale.[235] These early tests have again confirmed the efficacy of MNPCs, and show that with a small boost in efficiency they would be as effective as traditional toxic techniques utilising H_2O_2.

There are still some unanswered questions to their function, with competing separator design (magnet orientation, location, attempts to make the process continuous-flow are complex *etc.*) being one of the smaller concerns.[236] Moreover, the stability of MNPCs is still in question. Although nanosheets themselves offer better chemical and photo-stability than their microscopic counterparts, this is often not well characterised within previous literature reviewing MNPCs. Simply put, many are touted as ''stable'' over repeated cycles, but with no supporting evidence as to whether this is the case.[237] Macro-ZnO for example, is usually prone to photocorrosion, but is generally stable at the nano-scale. Nonetheless, photo-stability remains a concern across the board, and as VLA photocatalysis has been demonstrated with MNPCs utilising a wide range of materials,[236,238] this system remains a promising technique.

6.3 A combined approach

Previously discussed PCs are either immobilised on a solid or porous substrate, or used in suspension. Another approach would be to immobilise the PC onto a substructure which is then placed in suspension (see Fig. 20). This can be done to maximise mixing, and aid in the PC's retention or facilitate recovery. Some ways in which this approach can be applied are by; immobilising a PC on ceramic beads,[239,240] permeable hydrogel beads,[241–243] large inert carriers[238] or cilia-like constructions which are fixed on one end and allowed to move freely,[244] or forced to move using an external magnetic field.[245] Most of these systems which immobilise the PC onto a larger suspended particle will require further post processing similarly to a slurry style reactor, however this processing is simplified by the increased size of the PC and thus a coarser filter can be used for separation.

Zeolite has been experimented with for some time as a micro-scale TiO_2 carrier that when agitated within flow, releases TiO_2 which is then free for reactions, but also crucially reabsorbs TiO_2 when left to settle, allowing the TiO_2 to be recovered.[246] These systems may require post-process filtering stages or are challenging to synthesize, but eliminate the need for fine meshes or membranes, which reduces their cost. Leeching is also a problem with these systems, as certain carriers degrade over time (such as the UV degradation of hydrogels[242]), leading to possible contamination of the fresh-water output. Unfortunately, these methods, though better than static PCCs, still reduce the number of active sites and are therein less effective than suspended PCs.[247]

6.4 Photocatalytic reaction chambers (PRCs)

PRCs in practice vary in design depending on the light source, necessary recovery processes, immobilisation method, and the PC used. A non-exhaustive list of possible designs could be:

- A sunlight irradiated PRC, using a stirred vessel with internal walls coated in a PCC.
- A lamp driven, actively mixed PRC, which employs a MNPC. MNPCs would typically be used in batch processes, this could imply a high capital cost but would maximise the effectiveness of the photocatalyst.
- A UV-tube lamp surrounded by glass beads with PC immobilised on their surface.
- A sunlight irradiated membrane with PC incorporated into the membrane. Mirrors could be used to concentrate

Fig. 22 One of the first pilot plants for photocatalysis, employing a slurry reactor (in a static concentrator array) installed at latitude 40° (Arganda del Rey, Madrid, Spain). Costing estimates in Section 1 for plant scale PCs are taken from this plant's operation.[62] Reproduced with permission from ref. 67. Copyright 2002 Elsevier B.V.

sunlight onto the membrane surface. This could form a continuous flow, modular system.

- A sunlight irradiated tank utilising PC doped hydrogel beads which float and can be skimmed from the surface of the treated water.

Implementation thus dictates the design of the reactor, and its effectiveness.[248] Suspended PC reactors are much more active than immobilised systems, providing a near threefold improvement in degradation rate over contemporary PCCs.[249] Suspended reactors, often dubbed photocatalytic Slurry Reactors (SR, Fig. 22) are the most efficient method of applying PCs, yet operate on the assumption that the PC recovery process occurs elsewhere in the system, effectively separating the challenge of recovery and application. The numerical modelling of such photocatalytic systems can be extremely challenging[250] due to the combined effect of particle-fluid modelling (multi-phase flows) with combined radiation and chemical reaction modelling. Hence, full models examining steady-state PRC operation are largely in their infancy.[251]

Moving away from SR, there are a wide variety of PRCs designed to be implemented with PCCs and PMRs. Thin-film PRCs have been examined thoroughly, especially for use with immobilised[252] and suspended[253,254] PCs. These systems have largely fallen out of favour due to the generally low throughput and inherent drawbacks to immobilised photocatalysts.[249] Moreover, scaling these processes would require increasing footprint area, potentially making this system unfeasible for industry.

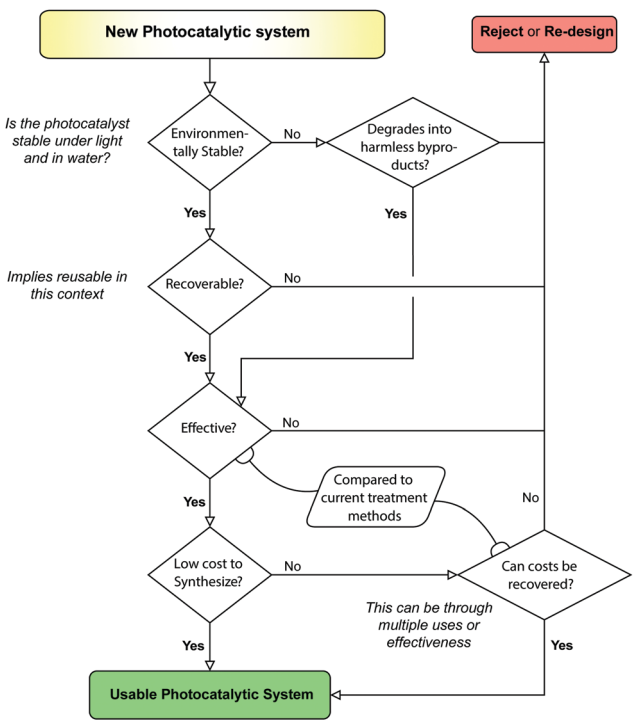

Fig. 23 The selection process for evaluating a PCS. A systems approach can consist of creating and evaluating a singular "system", or the creation of many modular "subsystems" which can work together to create a usable "system".

7 Recommendations for photocatalysis research

Throughout the writing of this review, the authors have come to several conclusions over what is best practice in the manufacture of photocatalytic composites. Foremost of these is a holistic view for PCs; Treatment, synthesis and recoverability should all be considered in unity when establishing the utility of a PC. This type of PC design is thus termed a Photocatalytic Systems (PCSs) approach (see Fig. 23). A PCSs view is key for both material synthesis and design, as well as certain recovery techniques, such as MNPCs and PMRs.

Environmental stability is one such factor which is consistently omitted from most papers, even though longevity and stability have a sizeable bearing on whether the system will be realistically worthwhile. TiO_2 is widely available simply because of this fact, appearing in a large chunk of the literature.[12] As P-25 is still in production, it proves low-cost and simple photocatalysts have their place in the market, but not yet widespread in industry. Putting effort into making a full product, from nanomaterial to device scales, can thus offset a number of hurdles for industrial adoption down the line.

A particular concern is an apparent lack of standardisation in solar-driven photocatalytic materials research. This inhibits reproducibility, prevents direct comparisons between materials systems, and ultimately delays the translation of research for large-scale water treatment. Table 3 highlights a sample of recent publications on photocatalytic materials or systems. In just these seven publications, ten different model pollutants have been used, eight of which are known to have sensitisation effects.[139] No less than six different light sources, from 'Visible Light' to a commercial solar simulator, have been stated with varying levels of detail given. Additionally, each has different conventions for interpreting and displaying data, and differing time scales for pollutant removal. A common claim in much of the literature is a seemingly enormous % removal of pollutant which upon closer inspection appears to be simply a large % removal *via* adsorption and then a subsequent, smaller than claimed, photocatalytic degradation of pollutant. These inconsistencies between experiments lead to a number of suggestions for future photocatalytic materials research:

(1) Light source and intensity be properly documented including the type of light and its intensity at the photocatalyst. Solar photocatalysis is a sustainable route forwards and as such the spectrum of the used light should be provided and compared to that of natural sunlight. Where possible light intensity at the catalyst should be equal to approximately 1 Sun. If possible, light should be collimated and if not this should be documented.

(2) Pollutants used should inhibit a light sensitisation effect with the photocatalyst. Examples might include salicylic acid and phenol.[137] Ideally, pollutants which undergo different degradation pathways should be used to gain a holistic view of the degradation of different organic pollutants.

Table 3 Photocatalytic treatments, highlighting the range of pollutants and light sources used, and the variability in the measured values. These factors make it difficult to directly compare studies on different materials applications

Material	Immobilisation	Pollutant	Radiation	Efficacy	Source
Ag_3PO_4 doped MoS_2, ZIF-8, h-BN	16 wt% in 150 μm thick PVDF MMM, glass slide cast	Drimaren Orange (P2R)[a]	150 W halogen lamp placed near	Constant flow treatment. P2R removal efficiencies between feed and effluent streams of 89, 79, 98% in 80 minutes measured using UV spectrophotometer. No mention of allowing membranes to reach P2R adsorption equilibrium in dark conditions. 15 L of water was treated. Pseudo first order removal rates 0.02487, 0.04093, 0.06139	219
MoS_2TiO_2	In suspension	Methylene Blue (MB)[a], crystal violet (CV)[a], rhodamine B (RhB)[a], Methyl Orange (MO)[a]	Solar simulator (*Asahi Spectra HAL 320*)	≈92% removal of MB using 50 wt% MoS_2:TiO_2 including significant adsorption. Stated removal % is inclusive of adsorption and photocatalytic degradation. Degradation measured using UV-Vis spectrophotometer.	255
MoS_2g-C_3N_4	In suspension	*E. Coli*	Visible light[b]	Up to 99.99% sterilisation of *E. Coli* was observed with good repeatability (less than 0.23% decrease in efficiency after 6 cycles)	256
ZnS nanospheres	Activated carbon	Congo Red (CR)[a]	Visible light[b]	88% CR removal after 100 minutes inclusive of significant (37%) adsorption and photocatalytic degradation. Initial CR concentration 25 mg L. CR concentrations measured *via* UV-Vis spectrophotometer.	257
TiO_2	Dip coated onto Fe-PPG	Methyl Orange (MO)[a]	45 W fluorescent lamp	Removed up to 95.3% of MO in 60 minutes with 23.3 mg g MO TiO_2 adsorbed for a removal rate of 0.083. Initial pollutant concentration 20 mg L^{-1}. Pollutant concentrations measured using direct spectrophotometer (464 nm)	258
MoS_2TiO_2	Vacuum filtered onto PAN membrane	Rhodamine B (RhB)[a], Methyl Orange (MO)[a], rhodamine 6G (RG6)[a], Malachite Green (MG)[a], Methylene Blue (MB)[a]	500 W xenon lamp 30 cm from liquid surface	Membranes allowed to float on water surface. Total fluid volume maintained at 50 mL by addition of DI water throughout. 83.88–97.73% removal of organic dye compounds from initial concentration 5 mg L^{-1} in 120 minutes. Pollutant adsorption unspecified however virgin PAN membrane showed 89.53% MB removal suggesting significant adsorption for all samples. No dark period to reach adsorption equilibrium is mentioned. Pollutant degradation measured *via* UV-Vis spectrophotometer.	221
MCU(DMSO)-C_3N_4	Vacuum filtered with PEG and GA cross linkers onto PVDF Membrane	Rhodamine B (RhB)[a], Tetracycline Hydrochloride (TC)	300 W Xenon lamp	Up to 84.24% removal of RhB in 250 minutes. Up to 71.26% removal of TC in 375 minutes. Initial pollutant concentrations were 5 mg L^{-1} and removal rates were 0.00748 and 0.00352 respectively. 1 hour of dark environment adsorption prior to photocatalytic effect but it is not mentioned if this is included in the final removal figures or not	222

[a] Organic dyes are known to have a photocatalytic sensitisation effect[150] (Table 2). [b] Unspecified – spectra unknown.

(3) Systems should be allowed to reach adsorption equilibrium, and measured periodically whilst in dark conditions to confirm that adsorption equilibrium has been reached. For constant flow membrane systems, the effluent should be recycled until a constant effluent pollutant concentration is reached under dark conditions. At which point the light should be turned on and the measurement of photocatalytic % degradation should be taken from the time the light is turned on instead of initial pollutant concentration in dark conditions.

(4) UV-Vis spectrophotometry can be used to determine the removal of compounds but it would be more rigorous to confirm these values, as well as the degradation of the initial pollutant and any degradation products, using methods such as thermogravimetric analysis and chemical oxygen demand.

8 Conclusions

Nanoscale photocatalyst materials are quintessentially one of many applications within water treatment (incl. nanoadsorbents & membrane nanotechnology, disinfection, sensing) where nanosheets are poised to play a major role in the

coming years.[202] 2D PCs in particular are gaining increased attention due to their increased quantum efficiency, surface area, facile construction of composites and crucially, their visible light active performance. Though the benefits of using 2D materials are well understood, scalable and sustainable routes to synthesis for many of the base 2D materials are lacking. These are required for manufacturing high performing photocatalytic composites at large scales. Most published research and patent-protected developments focus on the final PC, while those that focus on material synthesis struggle to balance high yields with defect-engineered nanosheet production. In most cases, a lack of standardisation for industry to adhere to has resulted in insufficient material quality that stymies progress in many fields using 2D materials, including sustainable photocatalysis. This highlights the critical need for material quality control and assurance methods to support with developments in international standardisation.

For applications in photocatalysis, scaling up production of nanomaterials is key for industrialised water treatment. Top-down methods have provided the primary synthesis for 2D semiconductors, charge carrier materials, and nanocomposites used in photocatalytic pollution remediation research. However, no single synthesis technique can address the breadth of photocatalytic materials possible. This highlights the importance for a variety of synthesis routes to be designed with considerations for sustainable and resource-efficient large-scale production and post-processing.

VLA-PCs are often constructed from a variety of different nanomaterials as composites, and though they are pioneering at the lab scale, they do not account for any systematic recovery of the composite essential for pilot plants. Development of new materials and composites which can maintain performance and permit easy removal and re-use is key. Even trading a little efficiency for facile separation is a worthwhile trade-off, as the costs for separating nanoparticles can be steep. Further materials research is necessary to achieve this balance, though a systems approach to these problems can guide research in the future. Modular approaches to PCs simply do not account for the entire life cycle of the photocatalyst, opting for a narrow view without addressing the factors preventing the adoption of nanosheet PCs.

Through writing this review, the authors have noted a marked difficulty in the comparison between different photocatalytic systems (Table 3 and Section 7). There are no well-defined metrics which allow for direct comparisons between photocatalytic systems such as PCCs, PMRs, PRCs *etc.* There have been rapid research developments focused on engineering VLA-PCs to achieve high pollution remediation efficiencies. This has grown the library of suitable 2D nanosheets and nanocomposite materials. However, this performance objective has been favoured over basic concerns of manufacture, stability and application, under the assumption that these issues can be addressed later. Due to the intertwined nature of synthesis, photocatalytic performance, application and recovery, more holistic approaches are necessary to engineer 2D photocatalysts for large-scale use. In summary, the main points barring the adoption of nanosheet PCs and others into water treatment are:

(1) Reduce the cost of nanosheet production while fully characterising the product – specific nanosheets required for VLA photocatalysts are prohibitively expensive. Lowering costs through production scaling will improve industrial accessibility for nanosheet-derived photocatalysts. This must be combined with accurate descriptions of the average nanosheet size including their length, width and number of layers along with their associated distributions and the typical lattice structure including any systematic defects present in the final material.

(2) Approach the design of nanosheet PCs at a systems level – nanosheet PCs are consistently designed without foresight towards their life-cycle. In order for them to be seen as a usable alternative to TiO_2, nanosheet PCs must be facile to synthesise and separate from inception, with PRCs being designed around their unique properties.

(3) Clearly state the stability of PCs over multiple cycles – most research discussing novel PCs (not exclusive to nanosheet-PCs) decline to provide any information on the stability of the PC in question, instead assuming inherent stability due to them being nano-sized. At a minimum, PCs should demonstrate sufficient stability so as to be cost effective with TiO_2-derived compounds. Standardisation across the research community would support this.

(4) Create simple, transferable metrics for comparing photocatalytic systems – many PC systems define throughput under differing conditions and metrics. This complicates comparisons between systems, and leaves a gap to derive standardised tests[259] and metrics for photocatalytic water treatment that can then be stated clearly when proposing new photocatalysts.

Nevertheless, solving these issues do not preclude the deployment of industrial water treatment. TiO_2-derived PCs have historically been much less effective in operation and slightly more expensive to set up when compared to other contemporary light absorption based AOPs (UV/O_3, UV/H_2O_2).[260] A shift to visible light absorbing, nanosheet-based PCs would close this gap; so long as material manufacture and recovery concerns are addressed.

Future research focus

Cost and real-world effectiveness are the primary reasons for the lack of competitive solar-driven photocatalytic systems today. To address these challenges, a number of key research focus areas and their corresponding Technology Readiness Level (TRL) are summarised in Fig. 24. Topics within TRL 1–5 should be considered holistically and with a systems thinking approach described previously (Fig. 23). Discovery and development of new photocatalytic materials and composites which are stable, maximise catalytic activity, and that can be produced on a large scale from abundant precursor sources will improve the cost and sustainability of nanosheet-based solutions. Similarly, scalable synthesis approaches with the ability to engineer material properties for targeted application-specific water treatments will be advantageous.

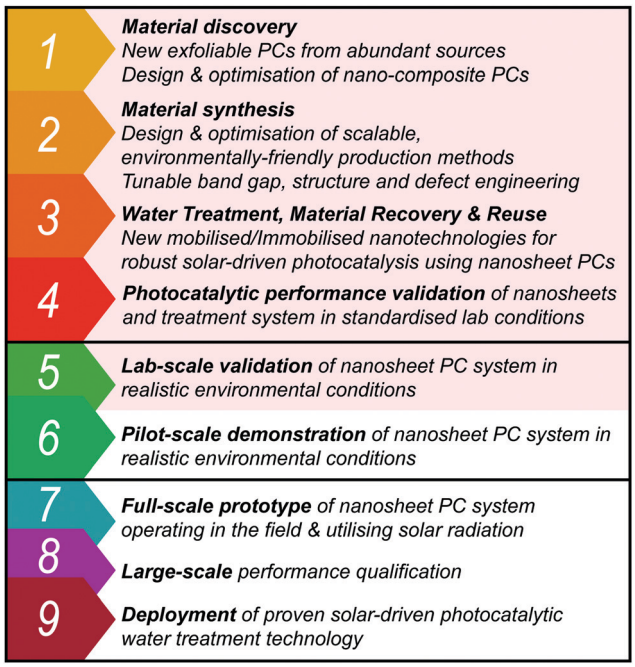

Fig. 24 Summary of future research focus areas according to Technology Readiness Level (TRL). Topics within TRL 1–4 align with the photocatalytic systems approach presented in Fig. 23. TRL 5 is highlighted as the prescribed TRL for laboratory research on solar photocatalytic water treatment to successfully transition to the pilot-scale demonstration stage in realistic environments.

On top of this, nanomaterial separation post-treatment remains a lasting issue, with some promising leads (MNPCs, membrane technology). Despite the recent work, significant effort is required to address this challenge and create a suite of viable solutions for material recovery and reuse. Nanotechnology advancements, either at the material discovery/synthesis level and/or the larger water treatment system level, are required to create efficient treatment and re-use processes that minimise operational and whole-life costs. A push towards greener treatment methods will be favourable for solar-driven photocatalysis, and with the correct incentives it can be made competitive with other AOPs.

Currently, the TRL for industrial scale photocatalytic water treatment systems is 5, as though some large scale demonstration plants have been made, most research is still focused on the small scale, seeking to push the boundaries of photocatalytic efficiency. Fundamental research efforts should continue, supported by the development of new standards for assessing photocatalytic performance using nanomaterials. This would ensure scientific repeatability and robust performance comparisons between different materials and devices.

The step between lab-scale validation and pilot-scale demonstration (TRL 5 to TRL 6) is non-trivial, however, a systems approach can ultimately lower the risk of a photocatalytic water treatment technology failing to progress beyond TRL 6. Pilot-scale demonstrations are often smaller than the full-scale prototype (TRL 7–9). Proving out the technology at this smaller pilot-scale may also open up other opportunities. Intensifying the passive nature of solar photocatalytic technology lends itself well to small, off-grid water purification strategies. Attempting to force photocatalysis to work at large scales is currently challenging, due primarily to how inexpensive other methods are in comparison, but also to a lesser extent the large footprint needed for a high-throughput system,[261] and the decreased effect they have against complex mixtures of organic pollutants in real wastewater.[262] Therefore, tailoring small scale photocatalytic reactors as air or water purifiers, could be another way to advance the commercialisation of fundamental research from TRL 1–5, allowing businesses to develop the viability of the technology and further strengthening the systems approach to designing nanomaterials for sustainable, solar-driven photocatalytic water treatment.

Abbreviations

SODIS	Solar water disinfection is a passive approach to water cleaning which kills pathogens *via* sunlight exposure
AOPs	Advanced oxidation processes are a subset of treatment techniques which produce highly reductive/oxidising species
PCs	Photocatalysts absorb light to directly catalyse reactions
VLA	Visible light active refers to the property of a PC to absorb within the visible light spectra
CPC	Compound parabolic concentrator
TOC	Total organic carbon
EC	Emerging contaminents
TMDs	Transitional metal dichalcogenides are transition metals covalently bonded to a chalcogenide pair
GO	Graphene oxide are graphene monolayers with high functionalisation
LPE	Liquid phase exfoliation is a subset of processes for constructing nanosheets dispersed in liquid
NPs	Nano-particles
PCCs	Photocatalytic coatings, where a photocatalyst is either coated directly onto a surface or immobilised in a carrier material such as a paint
FTO	Fluorine tin oxide, glass coated with a fluorine tin oxide layer to make it conductive
PMRs	Photocatalytic membrane reactors
MMMs	Mixed matrix membranes are a subset of photocatalytic membranes in which the photocatalyst is included within the material used to fabricate the membrane
MNPCs	Magnetic nano-photocatalysts
PRCs	Photocatalyitic reaction chambers
SR	Slurry reactors
NWs	Nano-wires
TDS	Total dissolved solids, a measure of the amount of dissolved material in a sample of water
HPC	Heterotrophic plate count, a procedure for estimating the number of live, culturable, heterotrophic bacteria in a water sample

rGO	Reduced graphene oxide
TRL	Technology readiness level
PCS	Photocatalytic systems

Author contributions

DP and JB: investigation, formal analysis, visualization and writing – original draft. EE, YM and HE: visualization and writing – review & editing. PD and JS: conceptualization, supervision, visualization and writing – review & editing.

Conflicts of interest

There are no conflicts to declare.

Acknowledgements

The authors acknowledge funding from the British Council Newton Fund – Institutional Links (Ref: 525463513). DP, JB and JS acknowledge funding from the EPSRC DTP (Ref: EP/T517926/1). JS also acknowledges funding from The Royal Society (Ref: RGS\R2 202379).

Notes and references

1 H. Ritchie, *Water Use and Stress*, 2017, **https://ourworldindata.org/water-use-stress**, (accessed November 2021).
2 A. G. Yehia, K. M. Fahmy, M. A. Mehany and G. G. Mohamed, *J. Water Clim. Change*, 2017, **8**, 484–494.
3 D. Conway, *Global Environ. Change*, 2005, **15**, 99–114.
4 D. L. Sedlak and U. von Gunten, *Science*, 2011, **331**, 42–43.
5 Progress on drinking water, sanitation and hygiene: 2017 update and SDG baselines, 2017, World Helath Organisation (WHO) and the United Nations Childrens Fund (UNICEF).
6 V. Gitis and N. Hankins, *J. Water Process Eng.*, 2018, **25**, 34–38.
7 J.-Q. Jiang, *Curr. Opin. Chem. Eng.*, 2015, **8**, 36–44.
8 J. Mansouri, S. Harrisson and V. Chen, *J. Mater. Chem.*, 2010, **20**, 4567–4586.
9 K. G. McGuigan, R. M. Conroy, H.-J. Mosler, M. du Preez, E. Ubomba-Jaswa and P. Fernandez-Ibañez, *J. Hazard. Mater.*, 2012, **235-236**, 29–46.
10 D. B. Miklos, C. Remy, M. Jekel, K. G. Linden, J. E. Drewes and U. Hübner, *Water Res.*, 2018, **139**, 118–131.
11 J. Schneider, D. Bahnemann, J. Ye, G. L. Puma and D. D. Dionysiou, *Photocatalysis: fundamentals and perspectives*, Royal Society of Chemistry, 2016.
12 B. Luo, G. Liu and L. Wang, *Nanoscale*, 2016, **8**, 6904–6920.
13 K. Sunada, Y. Kikuchi, K. Hashimoto and A. Fujishima, *Environ. Sci. Technol.*, 1998, **32**, 726–728.
14 Y. A. Attia and Y. M. A. Mohamed, *New J. Chem.*, 2022, **46**, 1677–1686.
15 B. Wang, B. Dong, M. Xu, C. Chi and C. Wang, *Chem. Eng. Sci.*, 2017, **168**, 90–100.
16 J. Ran, W. Guo, H. Wang, B. Zhu, J. Yu and S. Z. Qiao, *Adv. Mater.*, 2018, **30**, 1800128.
17 T. Oshima, D. Lu, O. Ishitani and K. Maeda, *Angew. Chem., Int. Ed.*, 2015, **54**, 2698–2702.
18 Q. Liu, H. Lu, Z. Shi, F. Wu, J. Guo, K. Deng and L. Li, *ACS Appl. Mater. Interfaces*, 2014, **6**, 17200–17207.
19 G. Zhang, C. D. Sewell, P. Zhang, H. Mi and Z. Lin, *Nano Energy*, 2020, **71**, 104645.
20 Y. Zhao, Y. Zhao, R. Shi, B. Wang, G. I. N. Waterhouse, L.-Z. Wu, C.-H. Tung and T. Zhang, *Adv. Mater.*, 2019, **31**, 1806482.
21 Y. M. A. Mohamed, H. A. E. Nazer, E. A. Elgohery and M. M. Khan, in *Chalcogenide-Based Nanomaterials as Photocatalysts*, ed. M. M. Khan, Elsevier, 2021, pp. 285–294.
22 W. Tu, Y. Zhou, Q. Liu, Z. Tian, J. Gao, X. Chen, H. Zhang, J. Liu and Z. Zou, *Adv. Funct. Mater.*, 2012, **22**, 1215–1221.
23 W. Tu, Y. Zhou, S. Feng, Q. Xu, P. Li, X. Wang, M. Xiao and Z. Zou, *Chem. Commun.*, 2015, **51**, 13354–13357.
24 Q. Xiang, B. Cheng and J. Yu, *Angew. Chem., Int. Ed.*, 2015, **54**, 11350–11366.
25 G. S. Shanker, A. Biswas and S. Ogale, *J. Phys.: Energy*, 2021, **3**, 022003.
26 D. Liu, S. Chen, R. Li and T. Peng, *Acta Phys.-Chim. Sin.*, 2021, **37**, 2010017.
27 R. A. Monteiro, C. Rodrigues-Silva, F. V. Lopes, A. M. Silva, R. A. Boaventura and V. J. Vilar, *Chem. Eng. J.*, 2015, **280**, 409–416.
28 B. L. Abrams and P. C. K. Vesborg, in *Catalysts for Environmental Remediation—Examples in Photo- and Heterogeneous Catalysis*, ed. S. L. Suib, Elsevier, 2013, pp. 63–85.
29 A. Rioja-Cabanillas, D. Valdesueiro, P. Fernández-Ibáñez and J. A. Byrne, *J. Phys.: Energy*, 2020, **3**, 012006.
30 Z. Wei, M. Xu, J. Liu, W. Guo, Z. Jiang and W. Shangguan, *Chin. J. Catal.*, 2020, **41**, 103–113.
31 V. L. Colvin, *Nat. Biotechnol.*, 2003, **21**, 1166–1170.
32 S. K. Loeb, P. J. J. Alvarez, J. A. Brame, E. L. Cates, W. Choi, J. Crittenden, D. D. Dionysiou, Q. Li, G. Li-Puma, X. Quan, D. L. Sedlak, T. David Waite, P. Westerhoff and J.-H. Kim, *Environ. Sci. Technol.*, 2019, **53**, 2937–2947.
33 Global Photovoltaic Power By Country, 2020, **https://solargis.com**, (accessed November 2021).
34 J.-M. Herrmann, *Appl. Catal., B*, 2010, **99**, 461–468.
35 A. Fujishima and K. Honda, *Nature*, 1972, **238**, 37–38.
36 J. Huang, X. Xu, C. Gu, G. Fu, W. Wang and J. Liu, *Mater. Res. Bull.*, 2012, **47**, 3224–3232.
37 G. R. Bamwenda and H. Arakawa, *Appl. Catal., A*, 2001, **210**, 181–191.
38 L. Zhang, W. Wang, J. Yang, Z. Chen, W. Zhang, L. Zhou and S. Liu, *Appl. Catal., A*, 2006, **308**, 105–110.
39 A. Harriman, J. M. Thomas, W. Zhou and D. A. Jefferson, *J. Solid State Chem.*, 1988, **72**, 126–130.
40 V. K. Saharan, D. V. Pinjari, P. R. Gogate and A. B. Pandit, *Advanced Oxidation Technologies for Wastewater Treatment*, Elsevier, 2014, pp. 141–191.
41 D. Vione, T. Picatonotto and M. Carlotti, *J. Cosmet. Sci.*, 2003, **54**, 513–524.

42 L. Chen, P. Xu and H. Wang, *J. Hazard. Mater.*, 2021, 127493.
43 A. Chauhan, M. Rastogi, P. Scheier, C. Bowen, R. V. Kumar and R. Vaish, *Appl. Phys. Rev.*, 2018, **5**, 041111.
44 J. Jing, M. Liu, V. L. Colvin, W. Li and W. W. Yu, *J. Mol. Catal. A: Chem.*, 2011, **351**, 17–28.
45 J. Schneider, M. Matsuoka, M. Takeuchi, J. Zhang, Y. Horiuchi, M. Anpo and D. W. Bahnemann, *Chem. Rev.*, 2014, **114**, 9919–9986.
46 W. Ho, J. Yu and S. Lee, *Chem. Commun.*, 2006, 1115–1117.
47 Y. Kondo, H. Yoshikawa, K. Awaga, M. Murayama, T. Mori, K. Sunada, S. Bandow and S. Iijima, *Langmuir*, 2008, **24**, 547–550.
48 H. An, B. Zhu, J. Li, J. Zhou, S. Wang, S. Zhang, S. Wu and W. Huang, *J. Phys. Chem. C*, 2008, **112**, 18772–18775.
49 L. Amirav and A. P. Alivisatos, *J. Phys. Chem. Lett.*, 2010, **1**, 1051–1054.
50 X. Yue, S. Yi, R. Wang, Z. Zhang and S. Qiu, *Nano Energy*, 2018, **47**, 463–473.
51 H. Rongan, L. Haijuan, L. Huimin, X. Difa and Z. Liuyang, *J. Mater. Sci. Technol.*, 2020, **52**, 145–151.
52 J.-H. Choy, H.-C. Lee, H. Jung, H. Kim and H. Boo, *Chem. Mater.*, 2002, **14**, 2486–2491.
53 Q. Lu, Y. Yu, Q. Ma, B. Chen and H. Zhang, *Adv. Mater.*, 2016, **28**, 1917–1933.
54 Q. Han, B. Wang, J. Gao, Z. Cheng, Y. Zhao, Z. Zhang and L. Qu, *ACS Nano*, 2016, **10**, 2745–2751.
55 J. Fu, Q. Xu, J. Low, C. Jiang and J. Yu, *Appl. Catal., B*, 2019, **243**, 556–565.
56 S. Leong, A. Razmjou, K. Wang, K. Hapgood, X. Zhang and H. Wang, *J. Membr. Sci.*, 2014, **472**, 167–184.
57 Y. Li, C. Gao, R. Long and Y. Xiong, *Mater. Today Chem.*, 2019, **11**, 197–216.
58 L. Wang, Z. Sofer and M. Pumera, *ACS Nano*, 2020, **14**, 21–25.
59 A. P. Kauling, A. T. Seefeldt, D. P. Pisoni, R. C. Pradeep, R. Bentini, R. V. B. Oliveira, K. S. Novoselov and A. H. Castro Neto, *Adv. Mater.*, 2018, **30**, 1803784.
60 ISO/TS 21356-1:2021(E), *Nanotechnologies – Structural characterization of graphene – Part 1: Graphene from powders and dispersions*, International Organization for Standardization Standard, 2021.
61 X. Li, J. Yu, S. Wageh, A. A. Al-Ghamdi and J. Xie, *Small*, 2016, **12**, 6640–6696.
62 A. Vidal, A. I. Díaz, A. E. Hraiki, M. Romero, I. Muguruza, F. Senhaji and J. González, *Catal. Today*, 1999, **54**, 283–290.
63 D. H. Quiñones, P. M. Álvarez, A. Rey and F. J. Beltrán, *Sep. Purif. Technol.*, 2015, **149**, 132–139.
64 A. Durán, J. Monteagudo, I. San Martín and S. Merino, *J. Environ. Manage.*, 2018, **210**, 122–130.
65 E. Moral Pajares, L. Gallego Valero and I. M. Román Sánchez, *Water*, 2019, **11**, 423.
66 B. Ohtani, O. Prieto-Mahaney, D. Li and R. Abe, *J. Photochem. Photobiol., A*, 2010, **216**, 179–182.
67 S. Malato, J. Blanco, A. Vidal and C. Richter, *Appl. Catal., B*, 2002, **37**, 1–15.
68 J. Ajona and A. Vidal, *Sol. Energy*, 2000, **68**, 109–120.
69 S. Malato, J. Blanco, D. C. Alarcón, M. I. Maldonado, P. Fernández-Ibáñez and W. Gernjak, *Catal. Today*, 2007, **122**, 137–149.
70 E. Casbeer, V. K. Sharma and X.-Z. Li, *Sep. Purif. Technol.*, 2012, **87**, 1–14.
71 B. Van der Bruggen, M. Mänttäri and M. Nyström, *Sep. Purif. Technol.*, 2008, **63**, 251–263.
72 H. Rajput, E. E. Kwon, S. A. Younis, S. Weon, T. H. Jeon, W. Choi and K.-H. Kim, *Chem. Eng. J.*, 2021, **412**, 128612.
73 H. Wu, H. L. Tan, C. Y. Toe, J. Scott, L. Wang, R. Amal and Y. H. Ng, *Adv. Mater.*, 2020, **32**, 1904717.
74 M.-Q. Yang, N. Zhang, M. Pagliaro and Y.-J. Xu, *Chem. Soc. Rev.*, 2014, **43**, 8240–8254.
75 M. Lu and P. Pichat, *Photocatalysis and Water Purification: From Fundamentals to Recent Applications*, John Wiley & Sons, Incorporated, Weinheim, Germany, 2013.
76 A. H. Castro Neto, F. Guinea, N. M. R. Peres, K. S. Novoselov and A. K. Geim, *Rev. Mod. Phys.*, 2009, **81**, 109–162.
77 A. K. Geim and K. S. Novoselov, *Nat. Mater.*, 2007, **6**, 183–191.
78 Y. Ebina, T. Sasaki, M. Harada and M. Watanabe, *Chem. Mater.*, 2002, **14**, 4390–4395.
79 M. Harada, T. Sasaki, Y. Ebina and M. Watanabe, *J. Photochem. Photobiol., A*, 2002, **148**, 273–276.
80 K. Nakata and A. Fujishima, *J. Photochem. Photobiol., C*, 2012, **13**, 169–189.
81 Y. Li, Y.-L. Li, B. Sa and R. Ahuja, *Catal. Sci. Technol.*, 2017, **7**, 545–559.
82 C. Daulbayev, F. Sultanov, B. Bakbolat and O. Daulbayev, *Int. J. Hydrogen Energy*, 2020, **45**, 33325–33342.
83 R. Frisenda, Y. Niu, P. Gant, M. Muñoz and A. Castellanos-Gomez, *npj 2D Mater. Appl.*, 2020, **4**, 38.
84 J. N. Coleman, M. Lotya, A. O'Neill, S. D. Bergin, P. J. King, U. Khan, K. Young, A. Gaucher, S. De, R. J. Smith, I. V. Shvets, S. K. Arora, G. Stanton, H. Y. Kim, K. Lee, G. T. Kim, G. S. Duesberg, T. Hallam, J. J. Boland, J. J. Wang, J. F. Donegan, J. C. Grunlan, G. Moriarty, A. Shmeliov, R. J. Nicholls, J. M. Perkins, E. M. Grieveson, K. Theuwissen, D. W. McComb, P. D. Nellist and V. Nicolosi, *Science*, 2011, **331**, 568–571.
85 V. Nicolosi, M. Chhowalla, M. G. Kanatzidis, M. S. Strano and J. N. Coleman, *Science*, 2013, **340**, 1226419.
86 A. K. Singh, K. Mathew, H. L. Zhuang and R. G. Hennig, *J. Phys. Chem. Lett.*, 2015, **6**, 1087–1098.
87 Y. Zhao, S. Zhang, R. Shi, G. I. Waterhouse, J. Tang and T. Zhang, *Mater. Today*, 2020, **34**, 78–91.
88 S. J. Moniz, S. A. Shevlin, D. J. Martin, Z.-X. Guo and J. Tang, *Energy Environ. Sci.*, 2015, **8**, 731–759.
89 K. Ren, K. Wang, Y. Cheng, W. Tang and G. Zhang, *Nano Futures*, 2020, **4**, 032006.
90 Z. Saleem, E. Pervaiz, M. U. Yousaf and M. B. K. Niazi, *Catalysts*, 2020, **10**, 464–499.
91 W.-J. Ong and K. P. Y. Shak, *Sol. RRL*, 2020, **4**, 2000132.
92 T. Su, Z. Qin, H. Ji and Z. Wu, *Nanotechnology*, 2019, **30**, 502002.

93 Y. Zhang, Z.-R. Tang, X. Fu and Y.-J. Xu, *ACS Nano*, 2011, **5**, 7426–7435.
94 K. Ren, J. Yu and W. Tang, *J. Alloys Compd.*, 2020, **812**, 152049.
95 H. Ji, P. Du, D. Zhao, S. Li, F. Sun, E. C. Duin and W. Liu, *Appl. Catal., B*, 2020, **263**, 118357.
96 H. A. El Nazer and Y. M. A. Mohamed, in *Chalcogenide-Based Nanomaterials as Photocatalysts*, ed. M. M. Khan, Elsevier, 2021, pp. 173–183.
97 H. S. Lee, S.-W. Min, Y.-G. Chang, M. K. Park, T. Nam, H. Kim, J. H. Kim, S. Ryu and S. Im, *Nano Lett.*, 2012, **12**, 3695–3700.
98 Z. Wang and B. Mi, *Environ. Sci. Technol.*, 2017, **51**, 8229–8244.
99 T.-F. Yeh, C.-Y. Teng, S.-J. Chen and H. Teng, *Adv. Mater.*, 2014, **26**, 3297–3303.
100 Y. Xia, B. Cheng, J. Fan, J. Yu and G. Liu, *Sci. China Mater.*, 2020, 1–14.
101 Z. Zhao, Y. Sun and F. Dong, *Nanoscale*, 2015, **7**, 15–37.
102 C. Lai, N. An, B. Li, M. Zhang, H. Yi, S. Liu, L. Qin, X. Liu, L. Li and Y. Fu, *et al.*, *Chem. Eng. J.*, 2020, 126780.
103 X. Zhang, Z. Zhang, D. Wu, X. Zhang, X. Zhao and Z. Zhou, *Small Methods*, 2018, **2**, 1700359.
104 H. L. Zhuang and R. G. Hennig, *J. Phys. Chem. C*, 2013, **117**, 20440–20445.
105 J. Zhang, P. Zhou, J. Liu and J. Yu, *Phys. Chem. Chem. Phys.*, 2014, **16**, 20382–20386.
106 L. Liu, H. Zhao, J. M. Andino and Y. Li, *ACS Catal.*, 2012, **2**, 1817–1828.
107 S. Pei and H.-M. Cheng, *Carbon*, 2012, **50**, 3210–3228.
108 Y. Zhu, S. Murali, W. Cai, X. Li, J. W. Suk, J. R. Potts and R. S. Ruoff, *Adv. Mater.*, 2010, **22**, 3906–3924.
109 T. Sreeprasad and V. Berry, *Small*, 2013, **9**, 341–350.
110 L. Vicarelli, S. J. Heerema, C. Dekker and H. W. Zandbergen, *ACS Nano*, 2015, **9**, 3428–3435.
111 N. Rono, J. K. Kibet, B. S. Martincigh and V. O. Nyamori, *J. Mater. Sci.: Mater. Electron.*, 2021, **32**, 687–706.
112 M. Najafi, A. Kermanpur, M. R. Rahimipour and A. Najafizadeh, *J. Alloys Compd.*, 2017, **722**, 272–277.
113 H. Safajou, H. Khojasteh, M. Salavati-Niasari and S. Mortazavi-Derazkola, *J. Colloid Interface Sci.*, 2017, **498**, 423–432.
114 X. Hu, P. Xu, H. Gong and G. Yin, *Materials*, 2018, **11**, 147.
115 I. Altin, X. Ma, V. Boffa, E. Bacaksz and G. Magnacca, *Mater. Sci. Semicond. Process.*, 2021, **123**, 105591.
116 H. V. Bao, N. M. Dat, N. T. H. Giang, D. B. Thinh, L. T. Tai, D. N. Trinh, N. D. Hai, N. A. D. Khoa, L. M. Huong, H. M. Nam, M. T. Phong and N. H. Hieu, *Surf. Interfaces*, 2021, **23**, 100950.
117 T. Govindaraj, C. Mahendran, V. S. Manikandan, J. Archana, M. Shkir and J. Chandrasekaran, *J. Alloys Compd.*, 2021, **868**, 159091.
118 H. Fattahimoghaddam, T. Mahvelati-Shamsabadi and B.-K. Lee, *J. Hazard. Mater.*, 2021, **403**, 123703.
119 A. H. Keihan, R. Hosseinzadeh, M. Farhadian, H. Kooshki and G. Hosseinzadeh, *RSC Adv.*, 2016, **6**, 83673–83687.
120 W. Lin, K. Lu, S. Zhou, J. Wang, F. Mu, Y. Wang, Y. Wu and Y. Kong, *Appl. Surf. Sci.*, 2019, **474**, 194–202.
121 M. Alomar, Y. Liu, W. Chen and H. Fida, *Appl. Surf. Sci.*, 2019, **480**, 1078–1088.
122 A. J. R. Luciano, L. de Sousa Soletti, M. E. C. Ferreira, L. F. Cusioli, M. B. de Andrade, R. Bergamasco and N. U. Yamaguchi, *J. Environ. Chem. Eng.*, 2020, **8**, 104191.
123 R. Atchudan, T. N. J. I. Edison, S. Perumal, M. Shanmugam and Y. R. Lee, *J. Photochem. Photobiol., A*, 2017, **337**, 100–111.
124 A. A. Yaqoob, N. H. B. Mohd Noor, A. Serrà and M. N. Mohamad Ibrahim, *Nanomaterials*, 2020, **10**, 932.
125 P. Gao, J. Liu, D. D. Sun and W. Ng, *J. Hazard. Mater.*, 2013, **250–251**, 412–420.
126 F. Wang, X. Yu, M. Ge, S. Wu, J. Guan, J. Tang, X. Wu and R. O. Ritchie, *Environ. Pollut.*, 2019, **248**, 229–237.
127 P. J. Sephra, P. Baraneedharan, M. Sivakumar, T. D. Thangadurai and K. Nehru, *Mater. Res. Bull.*, 2018, **106**, 103–112.
128 L. Wang, Q. Sun, Y. Dou, Z. Zhang, T. Yan and Y. Li, *J. Hazard. Mater.*, 2021, **413**, 125288.
129 A. M. Ramesh, A. Gangadhar, M. Chikkamadaiah, J. Krishnegowda and S. Shivanna, *J. Environ. Chem. Eng.*, 2020, **8**, 104071.
130 Y. Zhang, Y. Liu, P. Cheng, W. Song, X. Zhang, S. Rong, X. Gao, G. Zhou, Z. Zhang and J. Liu, *Chem. Eng. J.*, 2022, **430**, 132918.
131 H. Liu, Z. Chen, L. Zhang, D. Zhu, Q. Zhang, Y. Luo and X. Shao, *J. Phys. Chem. C*, 2018, **122**, 6388–6396.
132 Y. A. Attia, Y. M. A. Mohamed and T. A. Altalhi, *Desalin. Water Treat.*, 2016, **57**, 26014–26021.
133 Y. A. Attia and Y. M. A. Mohamed, *Appl. Organomet. Chem.*, 2019, **33**, e4757.
134 A. Irshad, F. Farooq, M. Farooq Warsi, N. Shaheen, A. Y. Elnaggar, E. E. Hussein, Z. M. El-Bahy and M. Shahid, *FlatChem*, 2022, **31**, 100325.
135 V. Thirumal, R. Yuvakkumar, P. S. Kumar, S. P. Keerthana, G. Ravi, D. Velauthapillai and B. Saravanakumar, *Chemosphere*, 2021, **281**, 130984.
136 H. Jing, Q. Cheng, J. M. Weller, X. S. Chu, Q. H. Wang and C. K. Chan, *J. Mater. Res.*, 2018, **33**, 3540–3548.
137 N. Barbero and D. Vione, *Environ. Sci. Technol.*, 2016, **50**, 2130–2131.
138 M. Grätzel, *Acc. Chem. Res.*, 2009, **42**, 1788–1798.
139 S. Malato, P. Fernández-Ibáñez, M. I. Maldonado, J. Blanco and W. Gernjak, *Catal. Today*, 2009, **147**, 1–59.
140 F. Li, L. Cheng, J. Fan and Q. Xiang, *J. Mater. Chem. A*, 2021, **9**, 23765–23782.
141 H. Wang, L. Zhang, Z. Chen, J. Hu, S. Li, Z. Wang, J. Liu and X. Wang, *Chem. Soc. Rev.*, 2014, **43**, 5234.
142 H. Wang, X. Li, X. Zhao, C. Li, X. Song, P. Zhang, P. Huo and X. Li, *Chin. J. Catal.*, 2022, **43**, 178–214.
143 J. Low, J. Ma, J. Wan, W. Jiang and Y. Xiong, *Acc. Mater. Res.*, 2022, **3**, 331–342.
144 Y. Bo, C. Gao and Y. Xiong, *Nanoscale*, 2020, **12**, 12196–12209.

145 Y. Li, X. Li, H. Zhang, J. Fan and Q. Xiang, *J. Mater. Sci. Technol.*, 2020, **56**, 69–88.
146 A. Serrà, L. Philippe, F. Perreault and S. Garcia-Segura, *Water Res.*, 2021, **188**, 116543.
147 V. Diesen and M. Jonsson, *J. Phys. Chem. C*, 2014, **118**, 10083–10087.
148 H. Tran Huu, M. D. N. Thi, V. P. Nguyen, L. N. Thi, T. T. T. Phan, Q. D. Hoang, H. H. Luc, S. J. Kim and V. Vo, *Sci. Rep.*, 2021, **11**, 14787.
149 S. Pasternak and Y. Paz, *Chem. Phys. Chem.*, 2013, **14**, 2059–2070.
150 S. Mozia, A. W. Morawski, R. Molinari, L. Palmisano and V. Loddo, *Photocatalytic membrane reactors: fundamentals, membrane materials and operational issues*, Elsevier, 2013, pp. 236–295.
151 Q. Xu, S. Wageh, A. A. Al-Ghamdi and X. Li, *J. Mater. Sci. Technol.*, 2022, **124**, 171–173.
152 Q. Xu, L. Zhang, B. Cheng, J. Fan and J. Yu, *Chem*, 2020, **6**, 1543–1559.
153 B. Chai, J. Yan, G. Fan, G. Song and C. Wang, *Chin. J. Catal.*, 2020, **41**, 170–179.
154 A. A. Daryakenari, B. Mosallanejad, E. Zare, M. A. Daryakenari, A. Montazeri, A. Apostoluk and J.-J. Delaunay, *Int. J. Hydrogen Energy*, 2021, **46**, 7263–7283.
155 Y. Liu, L. Ren, Z. Zhang, X. Qi, H. Li and J. Zhong, *Sci. Rep.*, 2016, **6**, 22516.
156 O. Akhavan, E. Ghaderi and R. Rahighi, *ACS Nano*, 2012, **6**, 2904–2916.
157 J.-Y. Lin, C.-Y. Chan and S.-W. Chou, *Chem. Commun.*, 2013, **49**, 1440.
158 K. K. Ghuman, S. Yadav and C. V. Singh, *J. Phys. Chem. C*, 2015, **119**, 6518–6529.
159 J. Xiong, J. Di, J. Xia, W. Zhu and H. Li, *Adv. Funct. Mater.*, 2018, **28**, 16163028.
160 H. Liu, S. Ma, L. Shao, H. Liu, Q. Gao, B. Li, H. Fu, S. Fu, H. Ye, F. Zhao and J. Zhou, *Appl. Catal., B*, 2020, **261**, 118201.
161 Y. Li, T. Liu, Z. Cheng, Y. Peng, S. Yang and Y. Zhang, *Chem. Eng. J.*, 2020, 127868.
162 C. Feng, L. Tang, Y. Deng, J. Wang, Y. Liu, X. Ouyang, H. Yang, J. Yu and J. Wang, *Appl. Catal., B*, 2021, **281**, 119539.
163 R. Shi, Y. Zhao, G. I. N. Waterhouse, S. Zhang and T. Zhang, *ACS Catal.*, 2019, **9**, 9739–9750.
164 K. R. Paton, E. Varrla, C. Backes, R. J. Smith, U. Khan, A. O'Neill, C. Boland, M. Lotya, O. M. Istrate, P. King, T. Higgins, S. Barwich, P. May, P. Puczkarski, I. Ahmed, M. Moebius, H. Pettersson, E. Long, J. Coelho, S. E. O'Brien, E. K. McGuire, B. M. Sanchez, G. S. Duesberg, N. McEvoy, T. J. Pennycook, C. Downing, A. Crossley, V. Nicolosi and J. N. Coleman, *Nat. Mater.*, 2014, **13**, 624–630.
165 A. Thomas, A. Fischer, F. Goettmann, M. Antonietti, J. O. Müller, R. Schlögl and J. M. Carlsson, *J. Mater. Chem.*, 2008, **18**, 4893–4908.
166 J. Fu, J. Yu, C. Jiang and B. Cheng, *Adv. Energy Mater.*, 2018, **8**, 1701503.
167 P. G. Karagiannidis, S. A. Hodge, L. Lombardi, F. Tomarchio, N. Decorde, S. Milana, I. Goykhman, Y. Su, S. V. Mesite, D. N. Johnstone, R. K. Leary, P. A. Midgley, N. M. Pugno, F. Torrisi and A. C. Ferrari, *ACS Nano*, 2017, **11**, 2742–2755.
168 J. Stafford, A. Patapas, N. Uzo, O. K. Matar and C. Petit, *AIChE J.*, 2018, **64**, 3246–3276.
169 R. Raccichini, A. Varzi, S. Passerini and B. Scrosati, *Nat. Mater.*, 2015, **14**, 271–279.
170 C. Tsakonas, M. Dimitropoulos, A. C. Manikas and C. Galiotis, *Nanoscale*, 2021, **13**, 3346–3373.
171 Y. Hernandez, V. Nicolosi, M. Lotya, F. M. Blighe, Z. Sun, S. De, I. McGovern, B. Holland, M. Byrne and Y. K. Gun'Ko, *et al.*, *Nat. Nanotechnol.*, 2008, **3**, 563–568.
172 K. D. Ausman, R. Piner, O. Lourie, R. S. Ruoff and M. Korobov, *J. Phys. Chem. B*, 2000, **104**, 8911–8915.
173 G. Cunningham, M. Lotya, C. S. Cucinotta, S. Sanvito, S. D. Bergin, R. Menzel, M. S. Shaffer and J. N. Coleman, *ACS Nano*, 2012, **6**, 3468–3480.
174 H. J. Salavagione, J. Sherwood, M. D. Bruyn, V. L. Budarin, G. J. Ellis, J. H. Clark and P. S. Shuttleworth, *Green Chem.*, 2017, **19**, 2550–2560.
175 M. Choucair, P. Thordarson and J. A. Stride, *Nat. Nanotechnol.*, 2009, **4**, 30.
176 Z. Li, R. J. Young, C. Backes, W. Zhao, X. Zhang, A. A. Zhukov, E. Tillotson, A. P. Conlan, F. Ding, S. J. Haigh, K. S. Novoselov and J. N. Coleman, *ACS Nano*, 2020, **14**, 10976–10985.
177 E. Varrla, K. R. Paton, C. Backes, A. Harvey, R. J. Smith, J. McCauley and J. N. Coleman, *Nanoscale*, 2014, **6**, 11810–11819.
178 J. N. Coleman, *Adv. Funct. Mater.*, 2009, **19**, 3680–3695.
179 J. N. Coleman, *Acc. Chem. Res.*, 2013, **46**, 14–22.
180 A. Ciesielski and P. Samori, *Chem. Soc. Rev.*, 2014, **43**, 381–398.
181 M. V. Bracamonte, G. I. Lacconi, S. E. Urreta and L. E. F. Foa Torres, *J. Phys. Chem. C*, 2014, **118**, 15455–15459.
182 C. Backes, T. M. Higgins, A. Kelly, C. Boland, A. Harvey, D. Hanlon and J. N. Coleman, *Chem. Mater.*, 2017, **29**, 243–255.
183 K. R. Paton, J. Anderson, A. J. Pollard and T. Sainsbury, *Mater. Res. Express*, 2017, **4**, 20531591.
184 N. Jeffers, J. Stafford, C. Conway, J. Punch and E. Walsh, *Exp. Fluids*, 2016, **57**, 17.
185 S. Biccai, S. Barwich, D. Boland, A. Harvey, D. Hanlon, N. McEvoy and J. N. Coleman, *2D Mater.*, 2019, **6**, 015008.
186 J. Stafford, N. Uzo, U. Farooq, S. Favero, S. Wang, H.-H. Chen, A. L'Hermitte, C. Petit and O. K. Matar, *2D Mater.*, 2021, **8**, 025029.
187 X. Yuan, C. Zhou, Y. Jin, Q. Jing, Y. Yang, X. Shen, Q. Tang, Y. Mu and A.-K. Du, *J. Colloid Interface Sci.*, 2016, **468**, 211–219.
188 F. Dong, Y. Li, Z. Wang and W.-K. Ho, *Appl. Surf. Sci.*, 2015, **358**, 393–403.
189 J. Ran, T. Y. Ma, G. Gao, X.-W. Du and S. Z. Qiao, *Energy Environ. Sci.*, 2015, **8**, 3708–3717.

190 P. Niu, L. Zhang, G. Liu and H.-M. Cheng, *Adv. Funct. Mater.*, 2012, **22**, 4763–4770.
191 C.-Y. Su, A.-Y. Lu, Y. Xu, F.-R. Chen, A. N. Khlobystov and L.-J. Li, *ACS Nano*, 2011, **5**, 2332–2339.
192 Y. Yang, H. Hou, G. Zou, W. Shi, H. Shuai, J. Li and X. Ji, *Nanoscale*, 2019, **11**, 16–33.
193 N. Liu, P. Kim, J. H. Kim, J. H. Ye, S. Kim and C. J. Lee, *ACS Nano*, 2014, **8**, 6902–6910.
194 J. Xu, L. Zhang, R. Shi and Y. Zhu, *J. Mater. Chem. A*, 2013, **1**, 14766–14772.
195 I. Papailias, N. Todorova, T. Giannakopoulou, N. Ioannidis, N. Boukos, C. P. Athanasekou, D. Dimotikali and C. Trapalis, *Appl. Catal., B*, 2018, **239**, 16–26.
196 A. M. Dimiev and J. M. Tour, *ACS Nano*, 2014, **8**, 3060–3068.
197 C. Hu, T. Lu, F. Chen and R. Zhang, *J. Chin. Adv. Mater. Soc.*, 2013, **1**, 21–39.
198 X. Huang, C. Tan, Z. Yin and H. Zhang, *Adv. Mater.*, 2014, **26**, 2185–2204.
199 J. S. Lee, K. H. You and C. B. Park, *Adv. Mater.*, 2012, **24**, 1084–1088.
200 C. Tan, J. Chen, X.-J. Wu and H. Zhang, *Nat. Rev. Mater.*, 2018, **3**, 20588437.
201 A. Reina, X. Jia, J. Ho, D. Nezich, H. Son, V. Bulovic, M. S. Dresselhaus and J. Kong, *Nano Lett.*, 2009, **9**, 30–35.
202 X. Qu, J. Brame, Q. Li and P. J. J. Alvarez, *Acc. Chem. Res.*, 2013, **46**, 834–843.
203 G. Panthi, M. Park, H.-Y. Kim, S.-Y. Lee and S.-J. Park, *J. Ind. Eng. Chem.*, 2015, **21**, 26–35.
204 B. Xu, M. B. Ahmed, J. L. Zhou, A. Altaee, G. Xu and M. Wu, *Sci. Total Environ*, 2018, **633**, 546–559.
205 M. Dijkstra, A. Michorius, H. Buwalda, H. Panneman, J. Winkelman and A. Beenackers, *Catal. Today*, 2001, **66**, 487–494.
206 B. Srikanth, R. Goutham, R. Badri Narayan, A. Ramprasath, K. Gopinath and A. Sankaranarayanan, *J. Environ. Manage.*, 2017, **200**, 60–78.
207 H. S. Russell, L. B. Frederickson, O. Hertel, T. Ellermann and S. S. Jensen, *Catalysts*, 2021, **11**, 20734344.
208 Y. Chen and D. Dionysiou, *Appl. Catal., B*, 2006, **69**, 24–33.
209 J. Zeng, S. Liu, J. Cai and L. Zhang, *J. Phys. Chem. C*, 2010, **114**, 7806–7811.
210 D. Sugiyana, M. Handajani, E. Kardena and S. Notodarmojo, *J. JSCE*, 2014, **2**, 69–76.
211 J. E. Duran, M. Mohseni and F. Taghipour, *AIChE J.*, 2011, **57**, 1860–1872.
212 R. Portela, S. Suárez, R. Tessinari, M. Hernández-Alonso, M. Canela and B. Sánchez, *Appl. Catal., B*, 2011, **105**, 95–102.
213 C. S. Turchi and D. F. Ollis, *J. Phys. Chem.*, 1988, **92**, 6852–6853.
214 N. S. Allen, M. Edge, G. Sandoval, J. Verran, J. Stratton and J. Maltby, *Photochem. Photobiol.*, 2005, **81**, 279–290.
215 M. T. Islam, A. Dominguez, R. S. Turley, H. Kim, K. A. Sultana, M. Shuvo, B. Alvarado-Tenorio, M. O. Montes, Y. Lin, J. Gardea-Torresdey and J. C. Noveron, *Sci. Total Environ.*, 2020, **704**, 135406.
216 M. Rani, Keshu, J. Yadav, Meenu and U. Shanker, *Environmental, legal, health, and safety issues of green nanomaterials*, Elsevier, 2022, pp. 567–594.
217 A. Bayat, M. Zirak and E. Saievar-Iranizad, *ACS Sustainable Chem. Eng.*, 2018, **6**, 8374–8382.
218 L. Ni, T. Wang, H. Wang and Y. Wang, *Chem. Eng. J.*, 2022, **429**, 132457.
219 A. V. Sonawane and Z. V. P. Murthy, *J. Membr. Sci.*, 2022, **641**, 119939.
220 S. A. Gokulakrishnan, G. Arthanareeswaran, Z. László, G. Veréb, S. Kertész and J. Kweon, *Chemosphere*, 2021, **281**, 130891.
221 X. Zhang, K. Fu and Z. Su, *Mater. Sci. Eng., B*, 2021, **269**, 115179.
222 J. Huang, J. Hu, Y. Shi, G. Zeng, W. Cheng, H. Yu, Y. Gu, L. Shi and K. Yi, *J. Colloid Interface Sci.*, 2019, **541**, 356–366.
223 T. Dou, L. Zang, Y. Zhang, Z. Sun, L. Sun and C. Wang, *Mater. Lett.*, 2019, **244**, 151–154.
224 P. Argurio, E. Fontananova, R. Molinari and E. Drioli, *Processes*, 2018, **6**, 162.
225 X. Chen, Y. Hu, Z. Xie and H. Wang, in *Materials and Design of Photocatalytic Membranes*, ed. A. Basile, S. Mozia and R. Molinari, Elsevier, 2018, book section 3, pp. 71–96.
226 S. Samsami, M. Mohamadi, M.-H. Sarrafzadeh, E. R. Rene, M. Firoozbahr, M. Mohamadizaniani and E. R. Rene, *Process Safety Environ. Protection: Trans. Insti. Chem. Eng., Part B*, 2020, **143**, 138–163.
227 I. Bellobono, B. Barni and F. Gianturco, *J. Membr. Sci.*, 1995, **102**, 139–147.
228 X. Zheng, Z. P. Shen, L. Shi, R. Cheng and D. H. Yuan, *Catalysts*, 2017, 7, 20734344.
229 W. Zhang, L. Ding, J. Luo, M. Y. Jaffrin and B. Tang, *Chem. Eng. J.*, 2016, **302**, 446–458.
230 C. Regmi, S. Lotfi, J. C. Espíndola, K. Fischer, A. Schulze and A. I. Schäfer, *Catalysts*, 2020, **10**, 2073–4344.
231 Y. S. Chung, S. B. Park and D.-W. Kang, *Mater. Chem. Phys.*, 2004, **86**, 375–381.
232 S. A. Heidari-Asil, S. Zinatloo-Ajabshir, O. Amiri and M. Salavati-Niasari, *Int. J. Hydrogen Energy*, 2020, **45**, 22761–22774.
233 B. Weng, M.-Y. Qi, C. Han, Z.-R. Tang and Y.-J. Xu, *ACS Catal.*, 2019, **9**, 4642–4687.
234 W. Wu, C. Jiang and V. A. L. Roy, *Nanoscale*, 2015, **7**, 38–58.
235 I. Sciscenko, S. Mestre, J. Climent, F. Valero, C. Escudero-Oñate, I. Oller and A. Arques, *Water*, 2021, **13**, 2073–4441.
236 J. Gómez-Pastora, S. Dominguez, E. Bringas, M. J. Rivero, I. Ortiz and D. D. Dionysiou, *Chem. Eng. J.*, 2017, **310**, 407–427.
237 M. Shekofteh-Gohari, A. Habibi-Yangjeh, M. Abitorabi and A. Rouhi, *Crit. Rev. Environ. Sci. Technol.*, 2018, **48**, 806–857.
238 Q. Wang, Q. Gao, A. M. Al-Enizi, A. Nafady and S. Ma, *Inorg. Chem. Front.*, 2020, **7**, 300–339.
239 Z. Isik, Z. Bilici, S. K. Adiguzel, H. C. Yatmaz and N. Dizge, *Environ. Technol. Innovation*, 2019, **14**, 100358.

240 N. Daneshvar, D. Salari, A. Niaei, M. H. Rasoulifard and A. R. Khataee, *J. Environ. Sci. Health, Part A: Toxic/Hazard. Subst. Environ. Eng.*, 2005, **40**, 1605–1617.
241 D. Xiong, W. Zhao, J. Guo, S. Li, Y. Ye, E. Lei and X. Yang, *Sep. Purif. Technol.*, 2021, **277**, 119628.
242 W.-H. Lam, M. N. Chong, B. A. Horri, B.-T. Tey and E.-S. Chan, *J. Appl. Polym. Sci.*, 2017, **134**, 26.
243 J. Feng, H. Ding, G. Yang, R. Wang, S. Li, J. Liao, Z. Li and D. Chen, *J. Colloid Interface Sci.*, 2017, **508**, 387–395.
244 D. Zhang, W. Wang, F. Peng, J. Kou, Y. Ni, C. Lu and Z. Xu, *Nanoscale*, 2014, **6**, 5516–5525.
245 M. Sun, Q. Wang, B. Dai, W. Sun, Y. Ni, C. Lu and J. Kou, *Energy Fuels*, 2020, **34**, 10290–10298.
246 G. Hu, J. Yang, X. Duan, R. Farnood, C. Yang, J. Yang, W. Liu and Q. Liu, *Chem. Eng. J.*, 2021, **417**, 129209.
247 M. N. Chong, B. Jin, C. W. Chow and C. Saint, *Water Res.*, 2010, **44**, 2997–3027.
248 A. Manassero, M. L. Satuf and O. M. Alfano, *Chem. Eng. J.*, 2017, **326**, 29–36.
249 A. Rachel, M. Subrahmanyam and P. Boule, *Appl. Catal., B*, 2002, **37**, 301–308.
250 Y. Boyjoo, M. Ang and V. Pareek, *Chem. Eng. Sci.*, 2013, **101**, 764–784.
251 J. Wang, B. Deng, J. Gao and H. Cao, *Chem. Eng. J.*, 2019, **357**, 169–179.
252 Y. Abdel-Maksoud, E. Imam and A. Ramadan, *Catalysts*, 2016, **6**, 2073–4344.
253 G. Li Puma and P. L. Yue, *Chem. Eng. Sci.*, 2003, **58**, 2269–2281.
254 G. Li Puma, *Chem. Eng. Res. Des.*, 2005, **83**, 820–826.
255 G. Chandrabose, A. Dey, S. S. Gaur, S. Pitchaimuthu, H. Jagadeesan, N. S. J. Braithwaite, V. Selvaraj, V. Kumar and S. Krishnamurthy, *Chemosphere*, 2021, **279**, 130467.
256 X. Zhang, F. Tian, X. Lan, Y. Liu, W. Yang, J. Zhang and Y. Yu, *Chem. Eng. J.*, 2022, **429**, 132588.
257 K. S. Bhavsar, P. K. Labhane, V. D. Murade, R. B. Dhake and G. H. Sonawane, *Inorg. Chem. Commun.*, 2021, **133**, 108958.
258 N. F. Aminuddin, M. A. Nawi, N. N. Bahrudin and A. H. Jawad, *Appl. Surf. Sci. Adv.*, 2021, **6**, 100180.
259 C. C. Le, M. K. Wismer, Z.-C. Shi, R. Zhang, D. V. Conway, G. Li, P. Vachal, I. W. Davies and D. W. C. MacMillan, *ACS Cent. Sci.*, 2017, **3**, 647–653.
260 N. N. Mahamuni and Y. G. Adewuyi, *Ultrason. Sonochem.*, 2010, **17**, 990–1003.
261 D. Spasiano, R. Marotta, S. Malato, P. Fernandez-Ibañez and I. Di Somma, *Appl. Catal., B*, 2015, **170-171**, 90–123.
262 J. J. Rueda-Marquez, I. Levchuk, P. Fernández Ibañez and M. Sillanpää, *J. Cleaner Prod.*, 2020, **258**, 120694.